Design of a Laboratory Test Bed for Planetary Rover Systems

by

Robert Daniel Burn III

Bachelor of Science in Mechanical Engineering
Massachusetts Institute of Technology (1997)

Submitted to the
Department of Mechanical Engineering
in partial fulfillment of the requirements for the degree of

Master of Science

at the

Massachusetts Institute of Technology

September, 1998

© 1998 Massachusetts Institute of Technology

Signature of Author _____
Department of Mechanical Engineering
August 7, 1998

Certified By _____
Steven Dubowsky
Thesis Supervisor

Accepted By _____
Ain A. Sonin
Chairman, Departmental Graduate Committee

MASSACHUSETTS INSTITUTE
OF TECHNOLOGY
JUL 1 2 1999
LIBRARIES
ENG

Design of a Laboratory Test Bed for Planetary Rover Systems

Submitted to the Department of Mechanical Engineering
on August 7, 1998, in partial fulfillment of the requirements for the degree of
Master of Science

by

Robert Daniel Burn III

Abstract

Robotic rovers are an important tool for scientists to explore and gather data from other planets. This thesis presents the design of an experimental test bed for studying planetary rover systems. The design of a six-wheeled rocker bogie rover and a mechanism for this rover to vary its geometry using shape memory alloys are presented. The rover's geometry is scaled from Jet Propulsion Laboratory's Lightweight Survivable Rover (LSR). The 3 degree of freedom manipulator arm and two end-effector designs are also detailed. These mechanisms are serving as the experimental system for studying control, vision, and planning issues of future rovers. Experimental results are presented for each design. From these results, future work and designs applicable to a Mars planetary rover are discussed.

Thesis Supervisor: Dr. Steven Dubowsky
Professor of Mechanical Engineering

Acknowledgements

I would like to thank Professor Dubowsky for giving me the opportunity to work in this research group. I appreciate his guidance and assistance with my education. I also would like to thank NASA and JPL for their support of this exciting project.

I would also like to thank my past and present colleagues and friends working on the NASA project. Shane Farritor, David Bevly, Herve Hacot, Vivek Sujan, Karl Iagnemma, Eric Wilhelm and Alvaro Rodriguez have provided invaluable help with my research. I also wish to thank the other members of the research group for making this an enjoyable experience.

Finally, I thank my friends and family for their encouragement and support.

Table of Contents

List of Figures

List of Tables

1 Introduction

1.1 Background

Planetary exploration is mankind's next frontier. Quests for life, land and resources have lured governments and scientists to our neighboring planet, Mars. On July 20, 1976, NASA's Viking Lander successfully landed on Mars, and transmitted back to earth images of the Red planet, such as the one seen in Figure 1.1. A 1.9 Kg meteorite believed to be from Mars was found on Antarctica, in 1993. This sample contained chemical traces that could have been of organic origin. This discovery sparked interest for more detailed exploration of Mars.

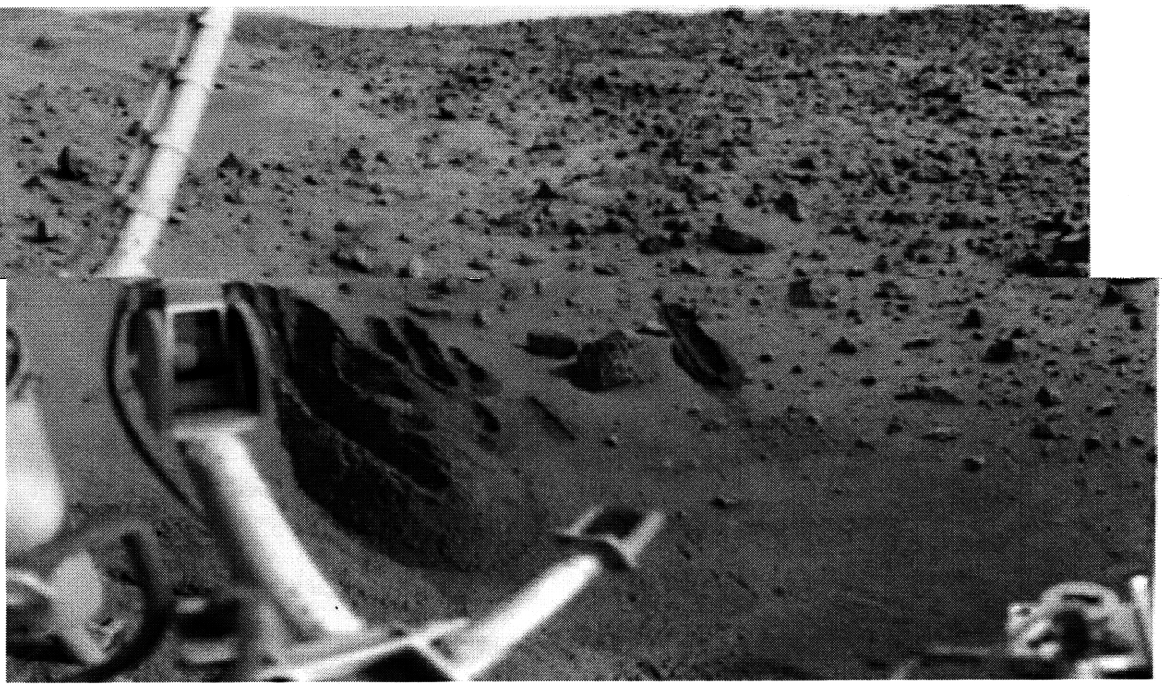

Figure 1.1: Viking Lander Mars Image (Viking Lander, 1976)

On July 4, 1997, the Mars Pathfinder mission landed the Sojourner rover on the surface of Mars (Golombek, 1998). This mission provided a means for the first successful teleoperation of a robot on Mars. Sojourner traversed 100 meters of terrain over 83 days, returned 550 images of the surface and performed spectral analysis of 15 rocks.

The success of Sojourner will soon be surpassed according to NASA's plan. Missions in 2001, 2003 and 2005 are scheduled to carry more rovers to Mars. The 2001 and 2003 proposed rovers have much more ambitious goals than Sojourner. These rovers will be designed to traverse up to 10 kilometers, last up to 1 year, manipulate and collect rock samples, and perform more detailed scientific tasks such as terrain mapping, digging, and drilling (Matijevic, 1997). The 2005 rover will collect the cache of rock samples collected by one of the two previous missions, and return to its landing craft, which will lift off from Mars and return the samples to earth. This sample return mission will allow for a much more detailed analysis of rocks than can be performed on board the rover.

1.2 Purpose of Research

This research has two purposes. The first purpose of this work is to develop an experimental test bed for planetary rover systems. In order to execute the '01 ,'03 and '05 missions, planetary rovers will need to have improved capability. These rover systems will be required to navigate more rugged terrain and travel much farther than Sojourner. First, the level of planning and control done on board the rover must be increased. Precise low level control of a rover through rough terrain cannot be done

through teleoperation with a several minute time delay. Second, the rover must be more able to physically adapt to its situation and terrain. The technology to achieve these improvements is being developed using the experimental system presented in this thesis. A planetary rover simulation has been developed based on physics based analysis of rover kinematics (Hacot, 1998). Based on this analysis, smart traction control algorithms have been developed using a fuzzy logic controller (Hacot, 1998). Extensive work has also been done on genetic algorithms for rover planning (Farritor, *et al.*, 1998).

The second purpose of my research is to develop new, lightweight mechanisms to increase the life span and capability of robotic planetary explorers. In order for future rovers to achieve long traverse distances, future mechanisms and capabilities will need to be very light weight to reduce power consumption. This thesis presents variable geometry mechanisms and new gripper designs for planetary rovers.

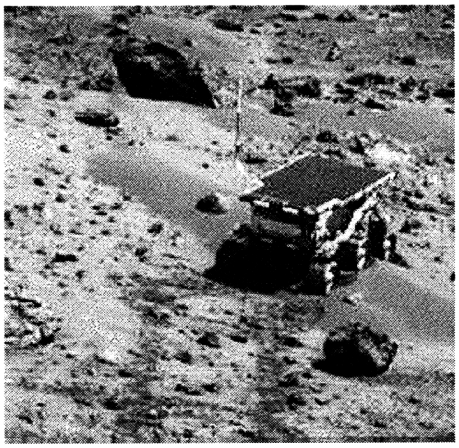

Figure 1.2: Sojourner Traversing Martian Terrain

1.3 Experimental System Overview

Figure 1.3 below shows the experimental system developed in this work. The system consists of a 6 wheel rover that is tethered to a desktop PC for power and control. A 3 degree of freedom manipulator is mounted to the front of the rover, which uses two prototype end-effector concepts for manipulation of rock samples. Also included in the experimental system, but not yet integrated, is a shape memory alloy (SMA) actuated mechanism for varying rover geometry. The next generation system, which is current laboratory work, will include low level control, analysis, planning, sensing, and power on board the rover. A wireless modem will eliminate the tether.

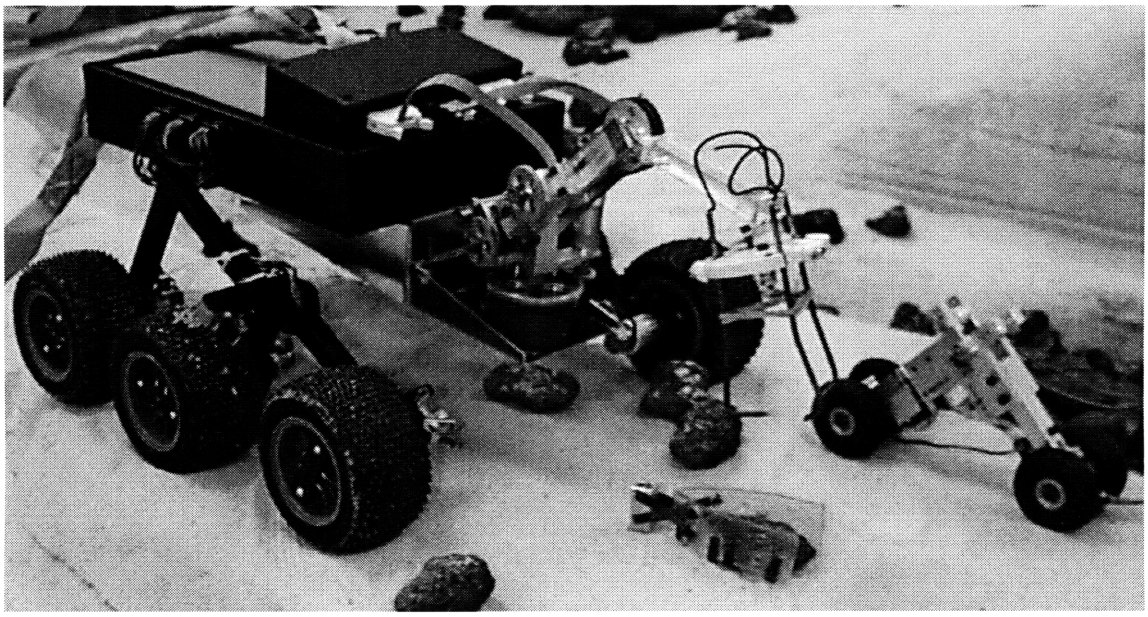

Figure 1.3: Experimental System

1.4 Outline of Thesis

Chapter 1 gives a background of planetary rover missions, both past and future as well as a purpose to and outline of this research. Chapter 2 discusses the background

and design of an experimental rover, as well as some experimental results. Chapter 3 details work done on an SMA actuated reconfigurability mechanism and presents results as well as a future design. Chapter 4 covers manipulator design and experimental results. Chapter 5 presents concepts for end-effectors and some results on grasping rock samples, and Chapter 6 contains some conclusions about this research and discusses future work.

2 Rover Design

2.1 Introduction

The experimental rover has 5 design requirements as shown in Table 2.1. The first requirement is that the rover design be similar to JPL's Lightweight Survivable Rover (Schenker, P., *et al.* (2)), which is an advanced design proposed for future missions. Second, the rover size must be compatible with the available laboratory space. An 8'x10' area is available for the rover to operate, so the rover must be small enough to have adequate room to operate. Third, the budget for this rover was approximately $10,000. The fourth requitement is that the rover be able to accomodate a manipulator and be self contained in the future. The fifth requirement is that the rover use as little power as possible, just like a real flight system. This chapter discusses the design of the rover. Section 2.2 describes rocker bogie design theory and presents JPL's LSR, which the experimental rover geometry is modeled after. The experimental mars yard in the laboratory is presented in section 2.3. Section 2.4 illustrates the rover design details, and Section 2.5 gives test results for the rover.

Table 2.1: Experimental Rover Requirements

	Functional Requirement	Design Parameter
1	Scaled Version of JPL's LSR	6 Wheels, Rocker Bogie
2	Size Compatible with Laboratory Space	About 12 inches long
3	Cost within Budget	Cost <$10,000
4	Able to Accommodate Manipulator and Self Containment Electronics	Have a Body and Arm Mounting Point
5	Low Power Usage	Lightweight and Highly Geared

2.2 Background

2.2.1 Rocker Bogie Design

The experimental system uses a six-wheel rocker-bogie design. In order to traverse rugged terrain, engineers at JPL have developed the rocker bogie vehicle, which has excellent mobility characteristics (Bickler, 1992). The vehicle features six independently powered wheels, suspended from a solid body. Each side of the vehicle has a rocker and a bogie, as seen in Figure 2.1. This design uses two freely pivoting joints on each side of the body, and rigid links. There are no springs or shock absorbers, as rovers will be moving slowly. The rocker pivots freely with respect to the rigid body. The rear wheel is mounted to one end of the rocker, and the bogie pivots freely about the other end. One wheel is mounted to each end of the bogie. A mirror image of the rocker and bogie is mounted on the other side of the body. A differential mounted in the body of the rover allows the body to split the difference of the two rocker angles.

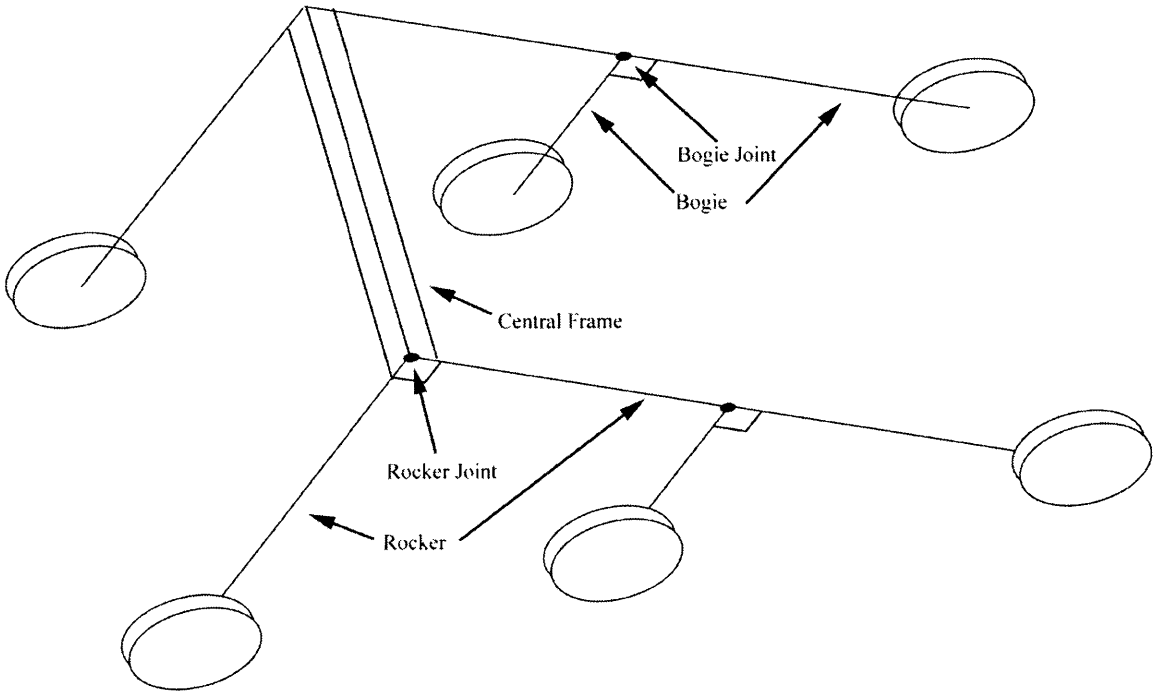

Figure 2.1: Rocker Bogie

This configuration has several advantages. The rocker bogie linkage causes a minimal displacement of the body when one wheel goes over a bump (Figure 2.2). For example, when the front wheel is lifted up one inch: the bogie pivot raises ½ inch, the rocker pivot raises ¼ inch, and the center of the body is only lifted 1/8 of an inch. Hence, this design allows for very high obstacles to be traversed with minimal body displacement, thus keeping the rover stable. Possibly the most significant advantage, however, is the rocker bogie's step climbing ability. With three motors per side, the weight is distributed so that the vehicle can climb a step that is larger than the radius of the wheel. For example, when the front wheel is climbing a face, the other two wheels can provide enough of a normal force on the front wheel so as not to slip on the wall.

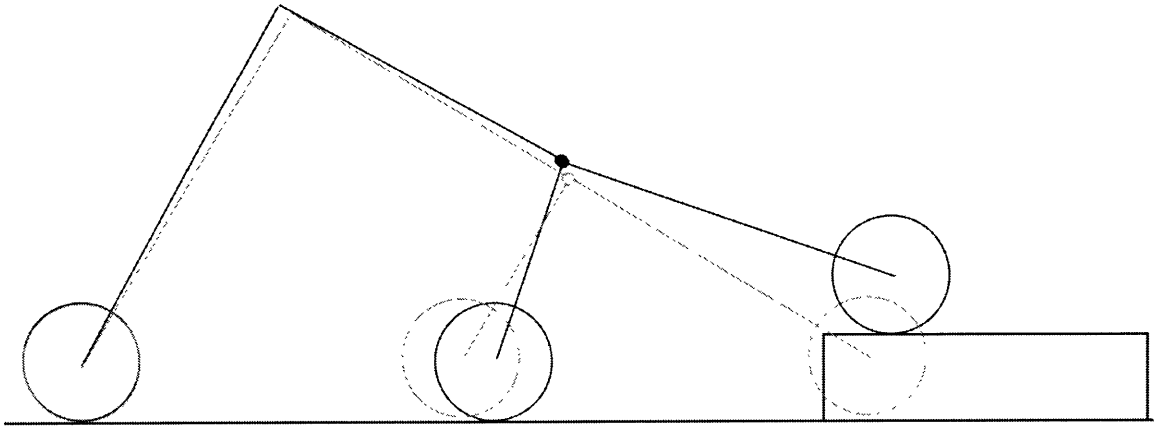

Figure 2.2: Rocker Bogie Displacement

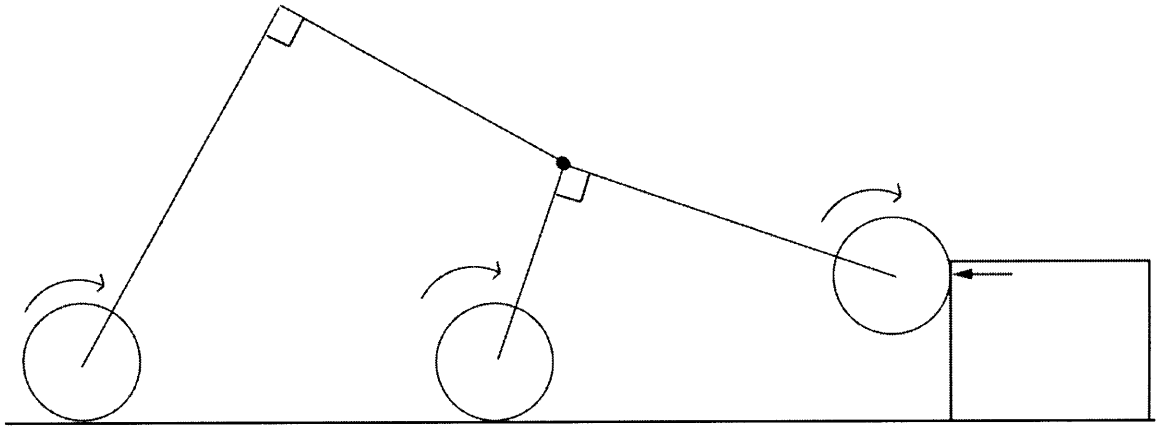

Figure 2.3: Rocker Bogie Climbing a Step

NASA used this rocker bogie design on Sojourner and is planning on using it on future sample acquisition rovers as well. JPL is developing a new rover design that takes advantage of the rocker bogie features even more than Sojourner did, called the LSR.

2.2.2 LSR

The LSR, or lightweight survivable rover, is an experimental system shown in Figure 2.4. It is constructed of composite materials to reduce weight, and has an integrated thermal-structural chassis. Perhaps the most innovative feature of this design is that the LSR can be stowed at only 30% of its operational volume. The linkages are

spring loaded to expand to their full size when mechanical restraints are released. The wheels collapse as well, as shown in Figure 2.5. Table 2.2 below, shows a comparison of Sojourner and the LSR. The LSR has over twice the ground clearance and can drive over much higher obstacles. In addition, the LSR is only 63% of Sojourner's weight, allowing it to carry 3 times the scientific payload weight (Schenker, P., *et al.* (2)).

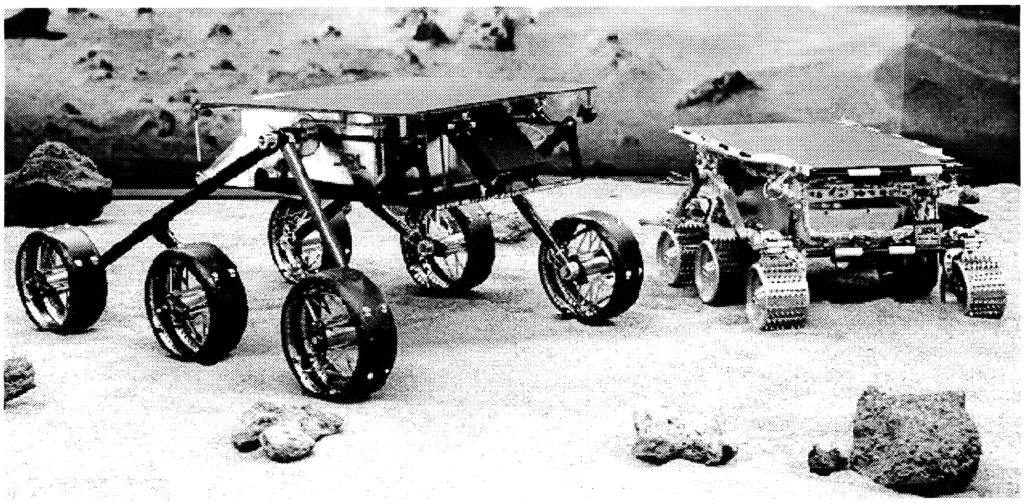

Figure 2.4: LSR (left) and Sojourner (Schenker, P., *et al.* (2))

Figure 2.5: LSR Collapsible Wheel (Schenker, P., *et al.* (2))

Table 2.2: LSR and Sojourner Data (Schenker, P., *et al.* (2))

	Sojourner	LSR-1
Dimensions, Operational (HxLxW)	280 mm x 630 mm x 480 mm	477 mm x 1000 mm x 728 mm
Stowed	72 liter (85 deployed)	<80 liter (325 deployed)
Mobility Type	6 wheel rocker bogie	6 wheel rocker bogie
Steering	ackerman steering, 4 wheels	skid steering
Speed	0.4 m/min	1.75 m/min
Wheel Diameter	130 mm	210 mm
Ground Clearance	130 mm	270 mm
Largest Obstacle	260 mm	350-400 mm
Obstacle Avoidance System	2 CCD camera, 5 laser stripe projector	2 CCD camera, 2 laser spot projector
Warm Electronics Box Interior	218 mm x 283 mm x 123 mm	300 mm x 300 mm x 150 mm
Thermal Control	25 mm silica aerogel, 3 W RHU	15 mm opacified aerogel, PCM panels
Interior Temperature Range	-40 to 40 C	-40 to 0 C
Power System	0.22 m2 GaAs solar array	0.25 m2 GaAs solar array
Battery	150 W-hr primary Li battery	30 W-hr rechargeable Li battery
Computer	80c85	80c85, upgrade to rad-hard 32 bit CPU
Telecommunications	UHF to lander	UHF to lander (or direct to orbiter)
Science	Alpha Proton X-ray Spectrometer	Multi-Spectral Imager, deployable tray, manipulator
Weight	10.4 Kg plus 1.1 Kg science	6.5 Kg plus up to 3.5 Kg science

2.3 Mars Test Bed

A key element to the experimental test bed is a Mars-like surface to test the rover. The MIT Field and Space Robotics Lab's (FSRL) rover simulation was run to determine what terrain would prove challenging for the rover (Hacot, 1998). From these results, an 8' by 10' terrain was designed and built in the laboratory, shown in Figure 2.6. The dimensions of the test area are based on laboratory floor space constraints. This test bed features hills with ±90° slope ranges, as well as 3 inch ditch depths. Sand, and small and large lava rocks were added as well.

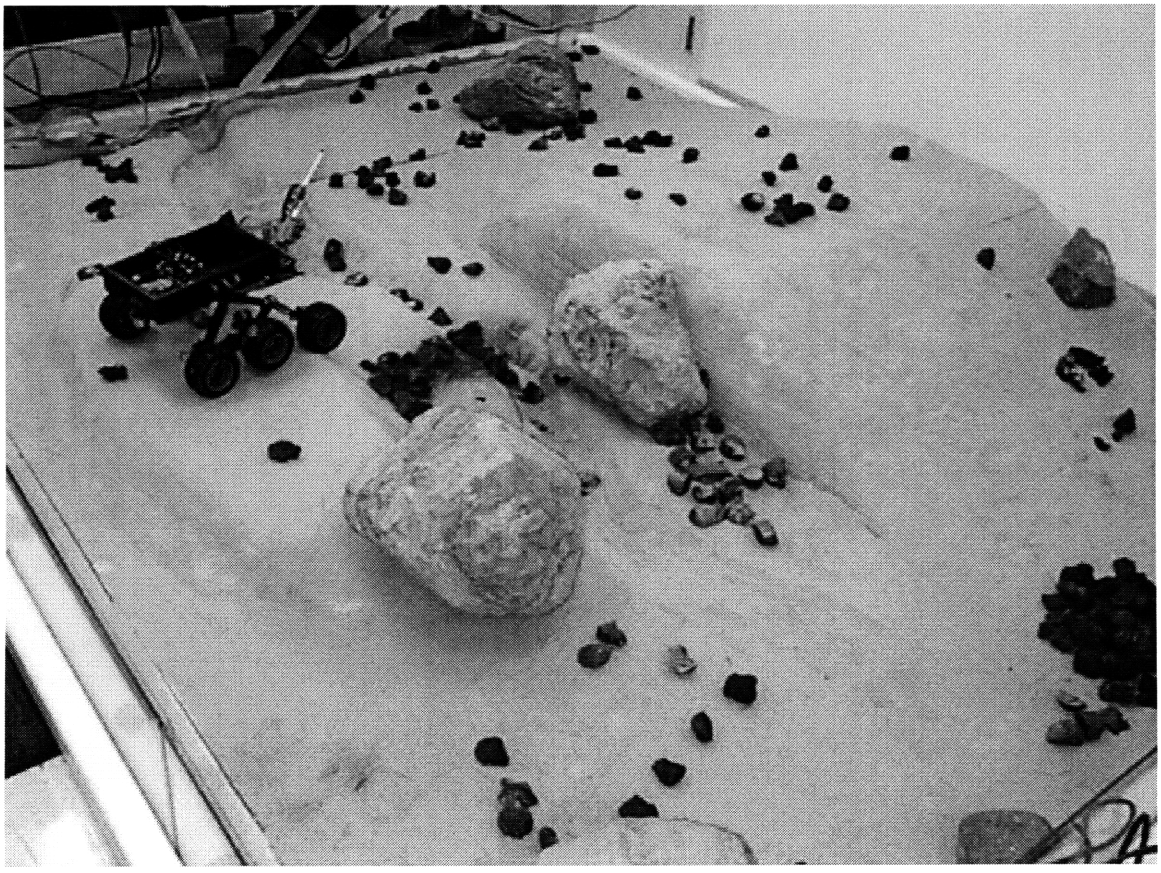

Figure 2.6: Mars Experimental Test Bed

2.4 Rover Design

The experimental rover's geometry was scaled after the LSR. Laboratory size constraints prohibit the rover from being 1 meter long like the LSR. Since the Mars test bed is 8 feet by 10 feet, a one foot long rover was chosen. This size allows for enough room to add an on board computer and battery, without being too large to move. Figure 2.7 shows a general schematic of the experimental design.

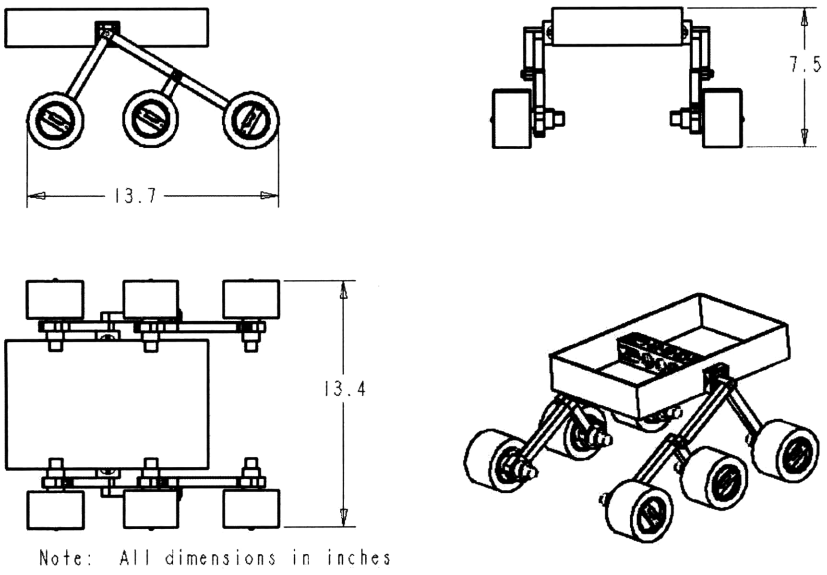

Figure 2.7: Experimental Rover Schematic

2.4.1 Structure Design

The structure of the rover is made of aluminum. The links are ½" square aluminum tubes with a 1/16" wall thickness. The joints are machined aluminum parts, with sealed ball bearings at the pivot points and can be seen in Figure 2.8. The backbone of the rover is the central frame that houses the differential and rocker pivot bearings. This frame is made of a 1" aluminum tube, to minimize deflection, with pockets

machined out to decrease weight. To contain future electronics and sensors, an aluminum box with 1/16" wall thickness is bolted to the rover frame. This enclosure also serves as an attachment point for the manipulator arm and a planned mast for scanning terrain ahead.

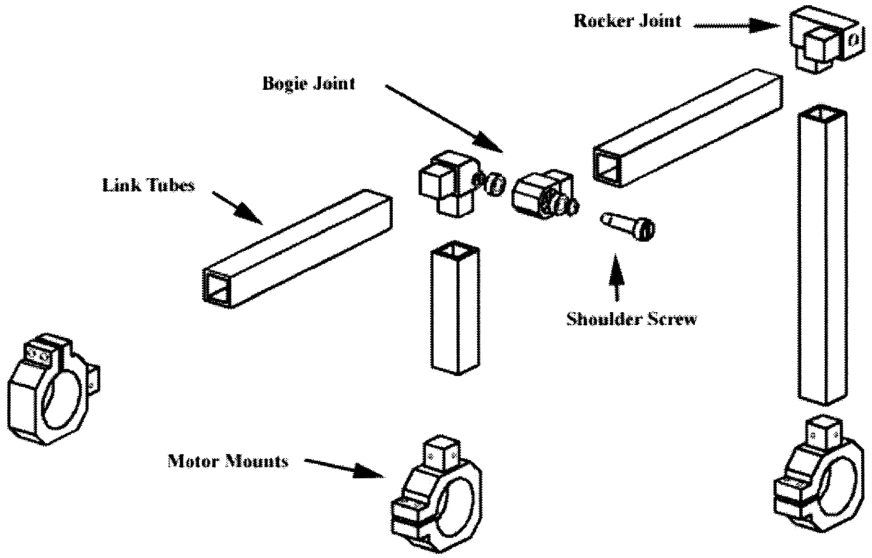

Figure 2.8: Rocker Bogie Exploded View

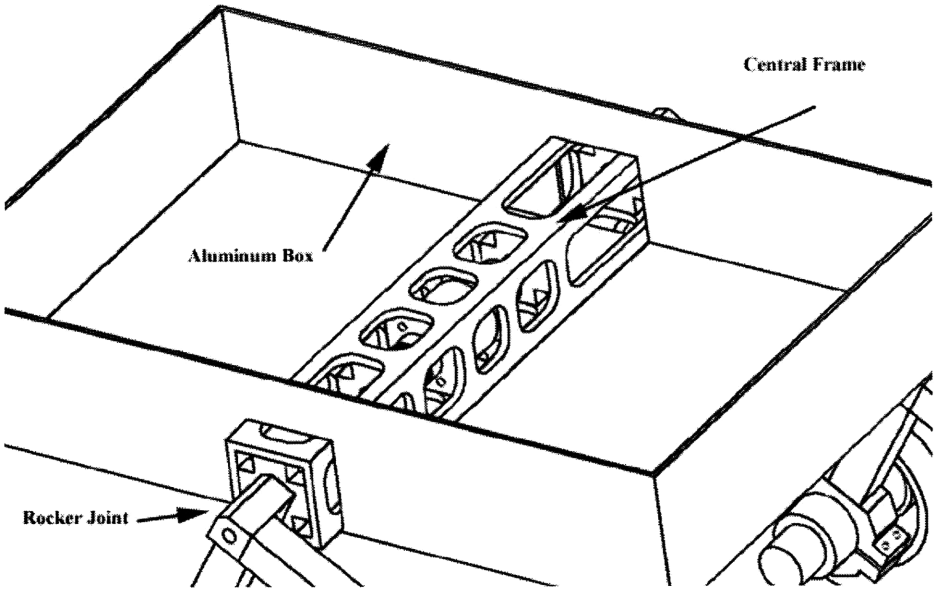

Figure 2.9: Rover Body

2.4.2 Motor Configuration

Each wheel of the rover is powered by its own motor. The motors must be highly geared to be able to exert a useful amount of torque while still being relatively small and light. A discontinued model of an Escap motor/gear head/tachometer combination was available at a very low price, and fit the rover requirements.

The first design challenge encountered was where to place the motors, and how to attach the wheels. Four different concepts were developed, as shown in Figure 2.10, and a concept selection chart was used to rate the concepts (Table 2.3).

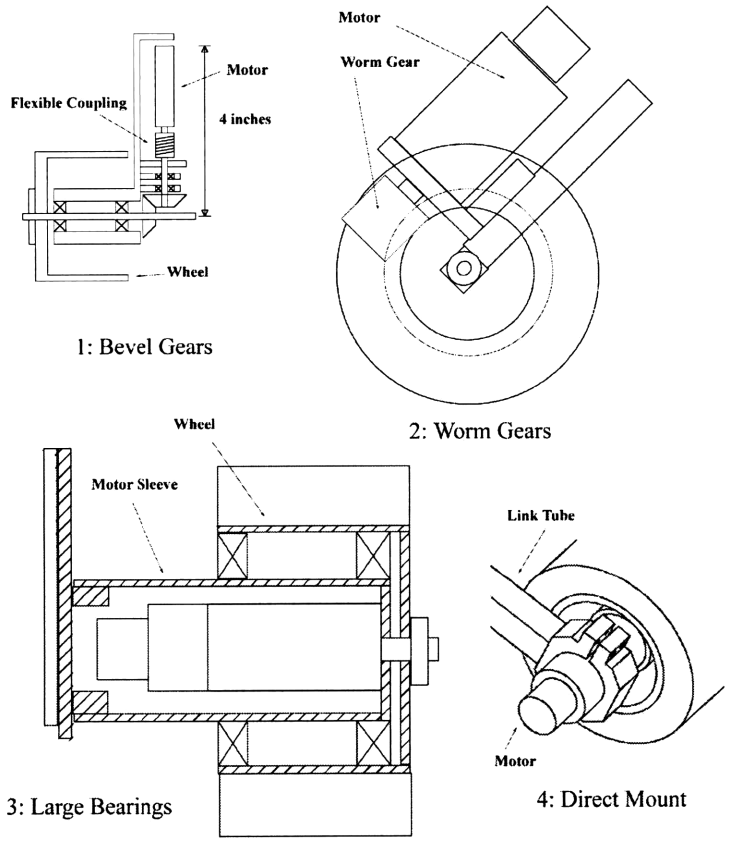

Figure 2.10: Motor Mount Concepts

Table 2.3: Motor Mount Concept Selection

				Motor Mount Concepts					
Selection Criteria	**Weight**	**1**		**2**		**3**		**4**	
		Bevel Gears (baseline)		**Worm Gears**		**Large Bearings**		**Direct Mount**	
	%	Rating	Weighted Score	Rating	Weighted Score	Rating	Weighted Score	Rating	Weighted Score
Weight	25	3	0.75	3	0.75	2	0 5	4	1
Complexity	20	3	0 6	2	0 4	2	0 4	4	0 8
Cost	10	3	0 3	3	0 3	2	0 2	5	0 5
Protect Motor	10	3	0 3	3	0.3	5	0 5	1	0 1
Sand Resistant	25	3	0 75	1	0 25	4	1	5	1 25
Ground Clearance	10	3	0 3	2	0 2	5	0 5	1	0 1
Total Score	**100**		**3**		**2.2**		**3.1**		**3.75**

Design 1 uses bevel gears to orient the motor perpendicular to the axis of the wheel. The advantages of this design is that the motors can be hidden inside the rocker bogie links. The disadvantages are that the bogie links must be long to fit the motors inside (making the rover 19+ in. length) and that ground clearance is hampered some by the protruding gears. Also, protecting the bevel gears from sand would add complexity to the design.

Design 2 solves the problem of long link lengths by using worm gears instead. This allows the motor axis to be offset from the wheel axis. However, worm gears are less efficient than spur or bevel gears because they are friction driven. This high friction also presents control problems. Also, sealing from sand would add even more complexity to this design.

Design 3 puts the motor inside the wheel (Farritor, 1997). This design improves ground clearance and requires no additional gears. Large diameter bearings take radial, axial and bending loads off of the gear head. A flexible coupling between the gear head shaft and the wheel design allows the two gear head bearings and the two wheel bearings

to co-exist on the same axis. One drawback to this design is increased weight. Reali-slim bearings from Kaydon with a 1.5" inner diameter weigh 0.6 ounces each. Twelve of these bearings would add up to an additional 7.5 ounces of weight. Also, thin walled bearing surfaces would add much complexity and machining time to the fabrication process. The most limiting problem, however, was that the wheel would have to be 3 ½ " wide to completely cover the motor. That would mean that each wheel would be over ¼ the width of the rover. This wheel width would not be to the same scale of the LSR.

Design 4 is the simplest design. The wheel is clamped to the gear head output shaft and the motor is held by a split clamp. This design requires only 3 parts (2 for the wheel clamp and one to hold the motor) and is the lightest design. One drawback is that ground clearance is hurt by the protruding motor and tachometer. The other drawback is that the load of the wheel must be supported by the gear head's bronze bushings. Using the worst case assumption that the maximum load on a single wheel could be half the weight of the rover, the projected moment on the gear head exceeds the manufacturer's recommendation by 11%. However, due to the low speed and infrequent operation of the rover's wheels, it is assumed that this limit can be exceeded slightly.

With all of the factors considered in the concept selection chart, design 4 was considered to be the most robust for experimental validation purposes. So far in 10 months of operation of the rover, not one gear head has broken due to wheel induced stress.

2.4.3 Differential

The body of the rover contains two bearings for each of the two rocker pivot shafts (see Figure 2.11). The differential is mounted along the axes of the shafts, in the center of the body frame tube. Including the two bearing surfaces in the differential, this configuration yields six bearings on a single axis. This over constrained design, therefore, requires two flexible couplings to allow for bearing misalignment, one on each side of the differential. The initial design of the rover used two helical aluminum flexures. These couplings compensate for axial and angular misalignment.

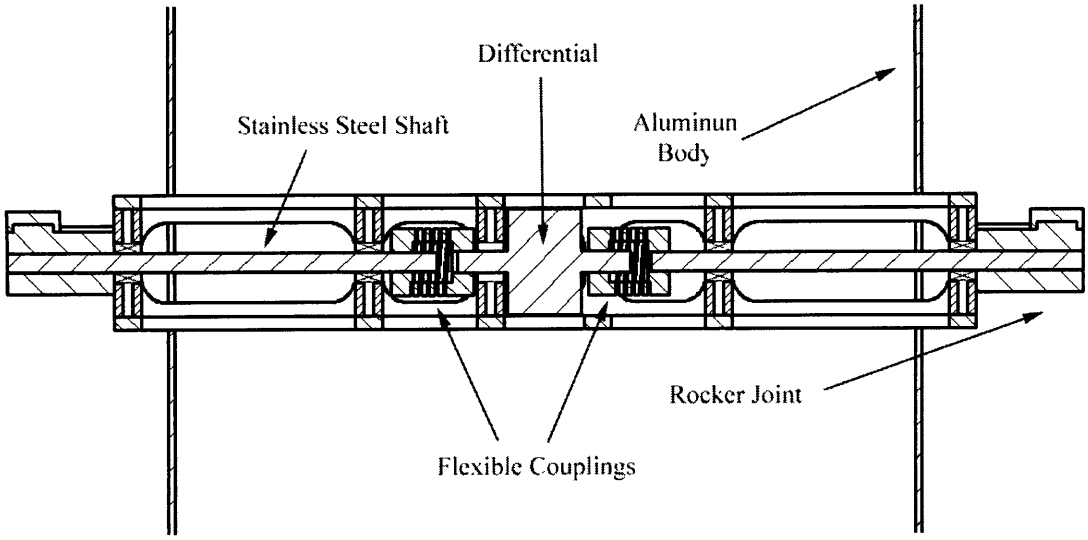

Figure 2.11: Rover Body Tube Cross-section

When the rover was assembled and tested, however, two problems became evident. The first problem was that the couplings slipped. Large torque induced by moderate forces on the front or rear end of the body caused the couplings to slip and the body to tilt up or down. The couplings could not be tightened to provide sufficient normal force without stripping the threads. The second problem was that the flexible

couplings were not stiff in torsion. The body would oscillate about the couplings at about 5 hertz, as the helical elements in the flexures behaved like weak springs.

Both of these problems were solved by replacing these flexible couplings with Uni-Lat© couplings from Small Parts Inc. (Figure 2.12). This coupling uses a universal joint design for angular misalignment with sliding pivots for radial misalignment. Because this design does not use flexures, it is very torsionaly stiff. Also, this design uses large diameter split clamps to keep the coupling from slipping under high torque.

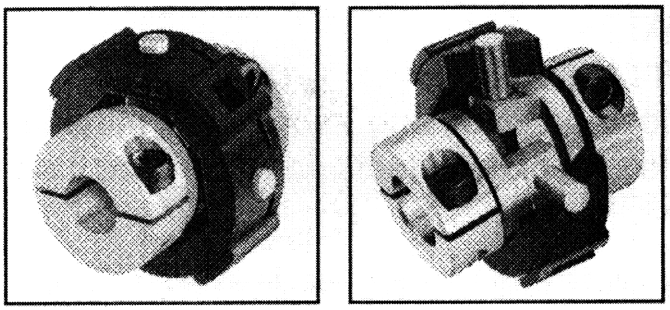

Figure 2.12: Uni-Lat© Couplings (Small Parts, 1997)

2.4.4 Sensors

The basic rover, without an arm or any self contained electronics, uses two types of sensors, one for wheel velocity and the other for rocker-bogie position. The motors use tachometers to sense motor velocity. They are cost-effective compared to optical encoders. Tachometers have two advantages over encoders in this case. First, they are smaller than optical encoders. Second, no special electronics are required to read them. The rotating tachometer produces a voltage proportional to its angular velocity. This voltage simply needs to be read by an A/D board. Encoders, however, allow for accurate position readings, and thus position control. Angular position can be obtained from a

tachometer by integrating velocity, but this reading is subject to drift, and therefore it is not very accurate. Soil-tire interactions, however, cause the wheels to slip. Therefore, it was decided that the exact angular wheel position is unnecessary.

In order to validate rover analysis, the rocker and bogie positions must be known. Therefore, potentiometers have been added to measure the angles of the rocker and bogie with respect to the body. Figures 2.13 and 2.14 show the mounting of these sensors. To measure the bogie angle, an aluminum coupling fastened to the shaft of the potentiometer is glued using silicone adhesive (so it can be removed easily) to the rotating shoulder bolt head on the bogie joint. The body of the potentiometer is fastened to the fixed rocker by an aluminum plate. Because very little torque is required to turn the potentiometer, deflection of the flat plate is negligible. To measure the rocker angles, a gear is pressed onto each rocker pivot shaft. A potentiometer with an identical gear pressed onto it, is then glued to the side of the frame tube. Although using two potentiometers in the body may be redundant in theory, there are several degrees of backlash in the differential which necessitates measurement of each rocker angle independently.

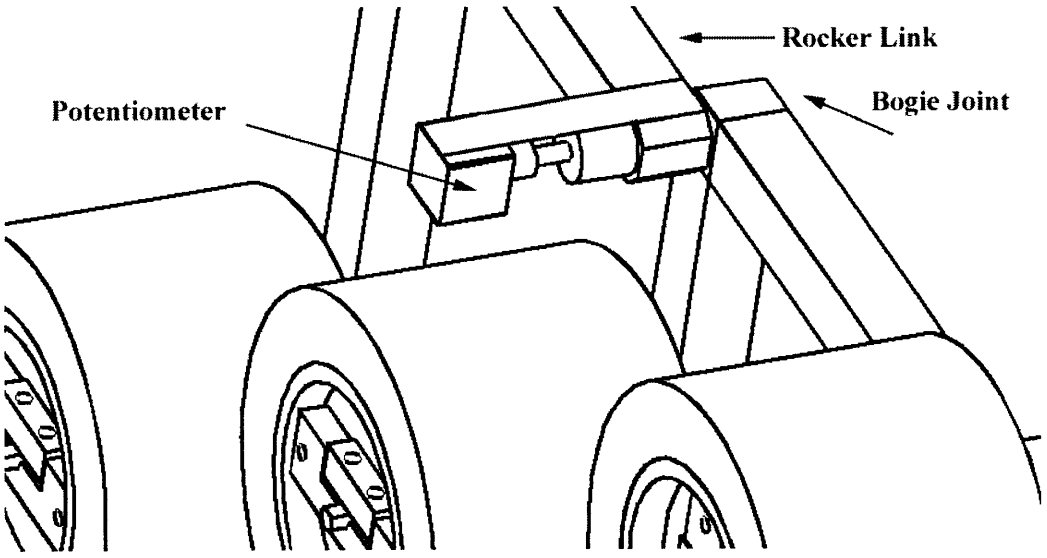

Figure 2.13: Bogie Potentiometer

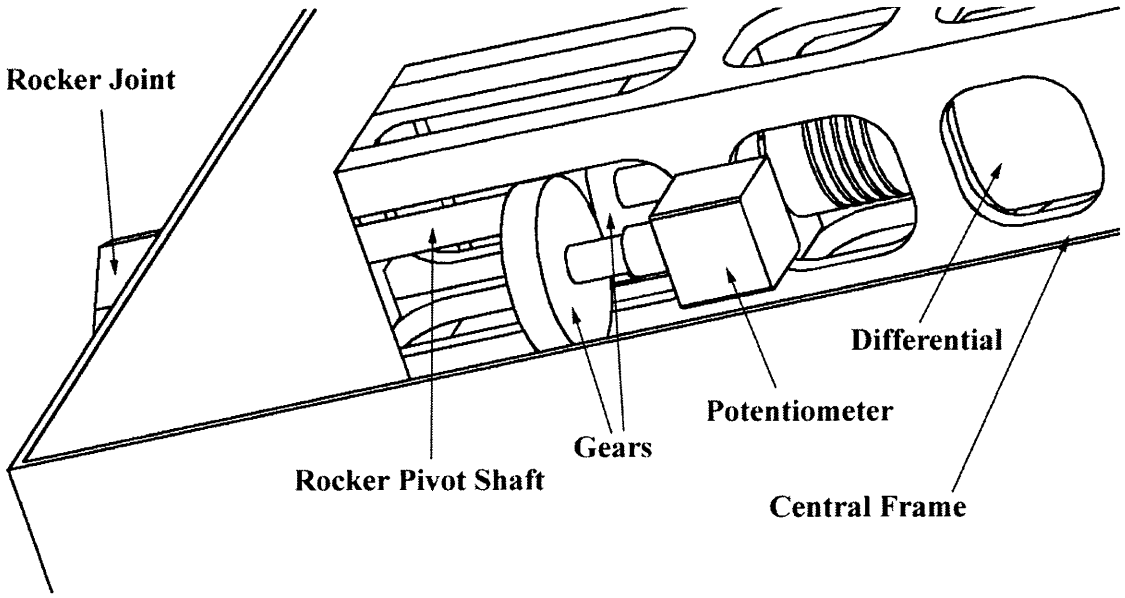

Figure 2.14: Rocker Potentiometer

2.5 Test results

Upon completion, the rover was tested. First tests were performed using PI velocity control on each wheel. Further work yielded a fuzzy logic controller which improved performance of the rover in certain tasks. Using the fuzzy logic controller, some baseline tests were performed on the rover to compare it to other planetary rovers. Table 2.4 shows a comparison of the rover with Sojourner and LSR. A step climbing test as well as a turning test were also performed. The rover was able to climb a maximum step height of 80 mm. At full speed, the rover was able to turn about its center (360 degrees) in 50 seconds.

Table 2.4: Rover Results

Sojourner	LSR-1	Mod 1
280 mm x 630 mm x 480 mm	477 mm x 1000 mm x 728 mm	191 mm x 348 mm x 340 mm
72 liter (85 deployed)	<80 liter (325 deployed)	23 liter (23 deployed)
10.4 Kg plus 1.1 Kg science	6.5 Kg plus up to 3.5 Kg scien	2.5 Kg
6 wheel rocker bogie	6 wheel rocker bogie	6 wheel rocker bogie
ackerman steering, 4 wheels	skid steering	skid steering
0.4 m/min	1.75 m/min	2.2 m/min
130 mm	210 mm	95 mm
130 mm	270 mm	146 mm
260 mm	350-400 mm	267 mm

Analysis has shown that the normal force of a wheel in contact with the ground could be changed by varying the torques of the other wheels (Hacot, *et al.*, 1998). The rover was used to confirm these tests. Figure 2.15 shows the data obtained from the tests. These results are presented and discussed in depth in (Hacot, *et al.*, 1998). The dashed lines represent predicted results while the solid lines show actual data. N_x is the normal force of the wheel in contact with the ground, and τ_x is the torque applied to the appropriate wheel. While the performance of the rover can be improved by control techniques that optimize performance based on a certain rover geometry, performance can also be improved by varying the rover's geometry, which is covered in the next chapter.

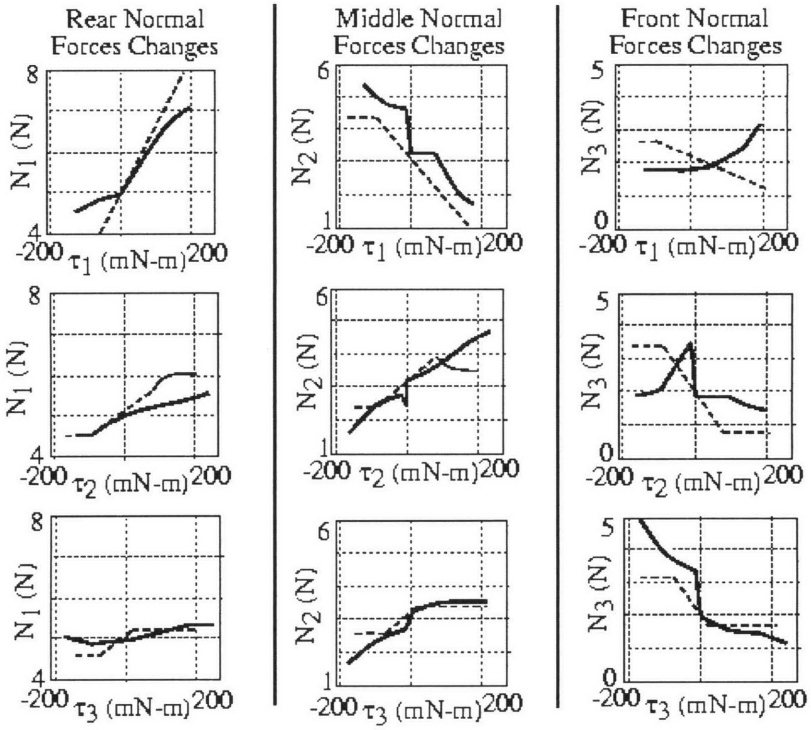

Figure 2.15: Traction Test Results (Hacot, *et al.*, 1998)

3 Reconfigurability

3.1 Introduction

This chapter presents work done to improve the mobility of a Mars exploration rover, thus decreasing the chance of mission failure. By increasing the amount of terrain that can be navigated, the rover will be able to select from a larger set of science objectives to investigate. The rover's mobility can be enhanced by giving it the capability to reconfigure its geometry.

The goals of a reconfigurability mechanism will be described in more detail in the next section. Section 3.3 discusses shape memory alloy actuation and its use in a reconfigurability system. Section 3.4 presents the design of the experimental reconfigurability system, with results in Section 3.5. Finally, a next generation design based on our experimental findings is covered in Section 3.6.

3.2 Motivation for Reconfigurability

The two most basic ways for a rocker bogie rover to vary its geometry are by changing the link lengths and by changing the rocker and bogie angles. Implementation of a reconfigurability mechanism will allow the rover to shift its weight to vary each wheel's traction with the ground, as well as increase the rover's stability for a given configuration.

During operation in rugged terrain, the rover could easily become trapped in a position that could lead to tipping. Unseen objects, crumbling terrain, or incorrect terrain

data can all lead to undesirable predicaments for the rover. One purpose of a reconfigurability mechanism is to allow the rover to squat one or both sides and increase its stability margin if it finds itself in a perilous position.

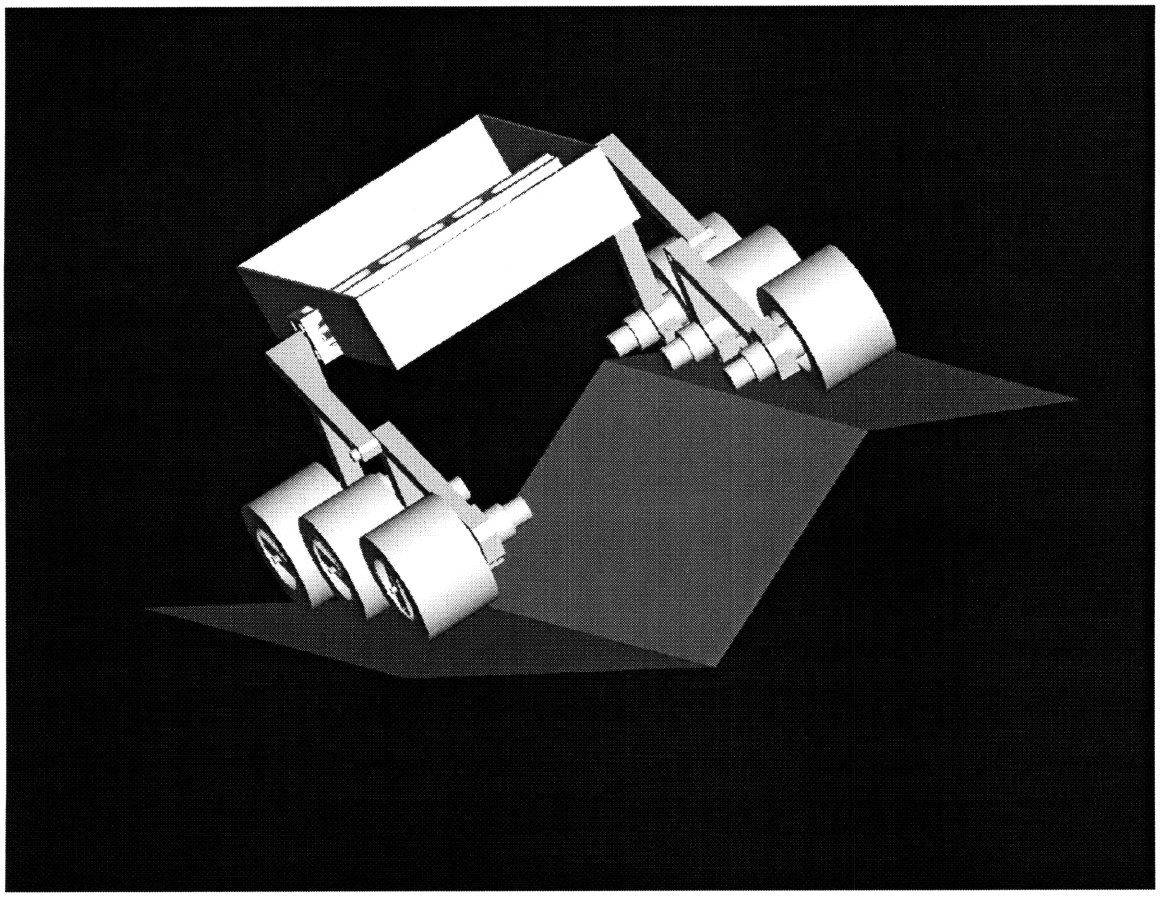

Figure 3.1: Rover Close to Tipping

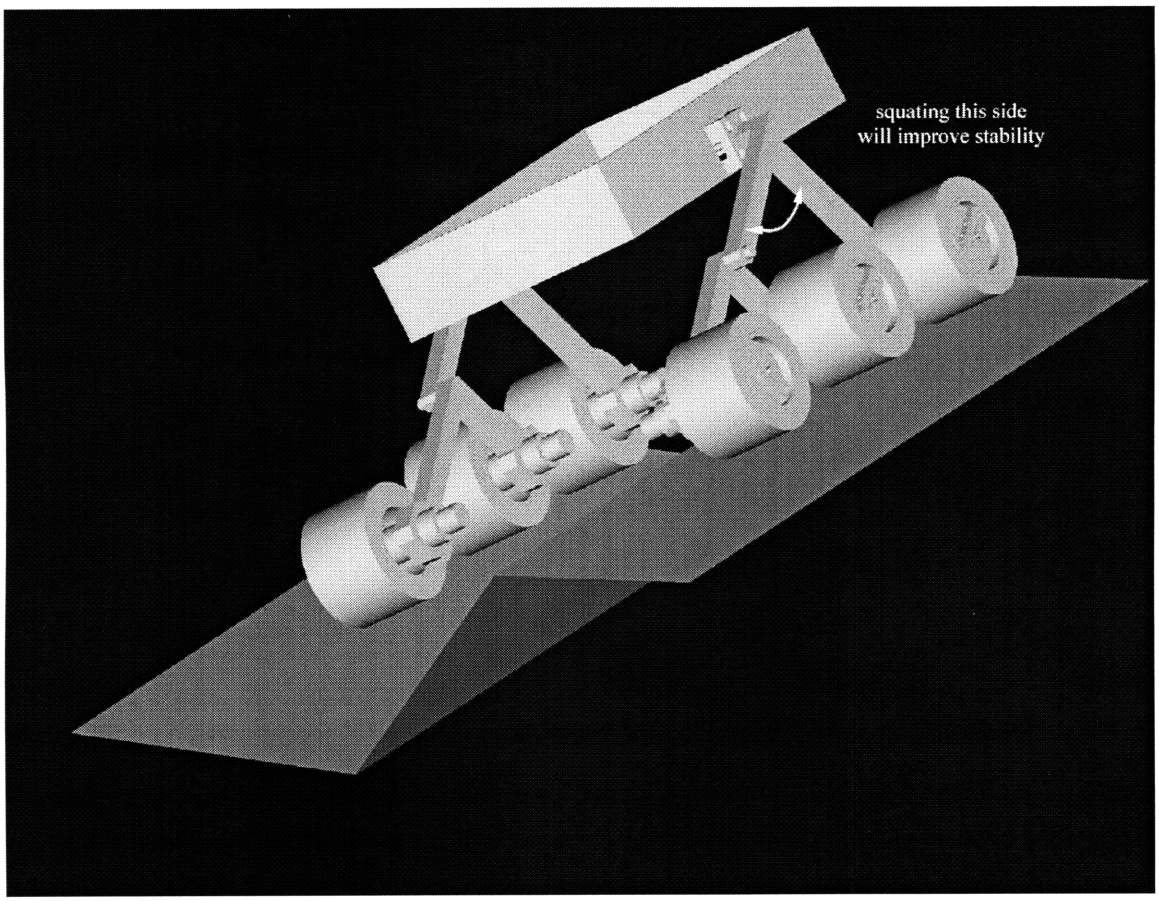

Figure 3.2: Squatting Left Side Increases Stability

In addition to increasing stability, the rover can shift its weight to perform traction control. When one wheel begins to slip, the rocker or bogie angle can be changed to move the center of mass vector closer to the wheel with the largest normal force vector in the direction of the center of mass vector.

3.3 Shape Memory Alloy Actuation

3.3.1 Background

The key element to the design of a variable geometry mechanism to change rocker or bogie angles is developing an appropriate actuator. The actuator must have a high force/weight ratio in order to keep the system lightweight. Planetary applications

limit the variety of actuator types. Hydraulic actuators, for example, can exert very high forces, but they have too many problems. Pumps, hoses and seals would increase weight, and keeping the fluid from freezing or leaking would add complexity as well. Pneumatics would have similar problems with pumps, seals and hoses. Electric solenoids would not be able to exert enough force, without consuming large amounts of power. The common method of actuation is a geared electric motor, but this adds weight, bulk and reliability problems to the design. Another possible, but less common, method of actuation is shape memory alloy. Due to its light weight and simplicity as an actuator, shape memory alloys actuation is being investigated for a reconfigurability mechanism.

3.3.2 SMA Properties

Shape memory alloys posses unique stress-strain properties. An SMA can be deformed plastically, and then returned to its original shape by being heated. The most common alloy is Nitinol (NiTi). A NiTi SMA is in its martensite phase at room temperature. When stressed, the martensite crystal structure slips causing up to 8% strain (Figure 3.3). When the alloy is heated above 68 °C, the alloy transforms into the austentite phase and its original crystal structure is restored. Figure 3.4 shows the stress-strain curves of the two different phases. This special alloy can be used as an actuator, because the ratio of the deformation stress to the actuated recovery stress can be higher than 10 to 1.

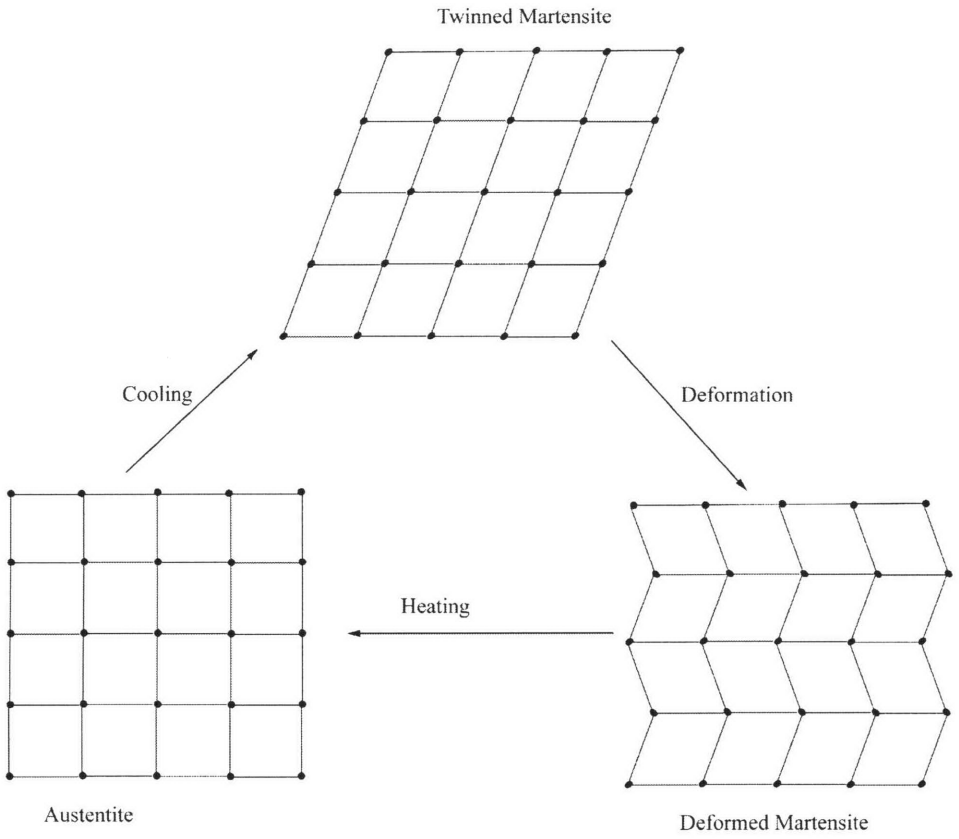

Figure 3.3: Austentite and Martensite Crystal Structures (Duerig, 1990)

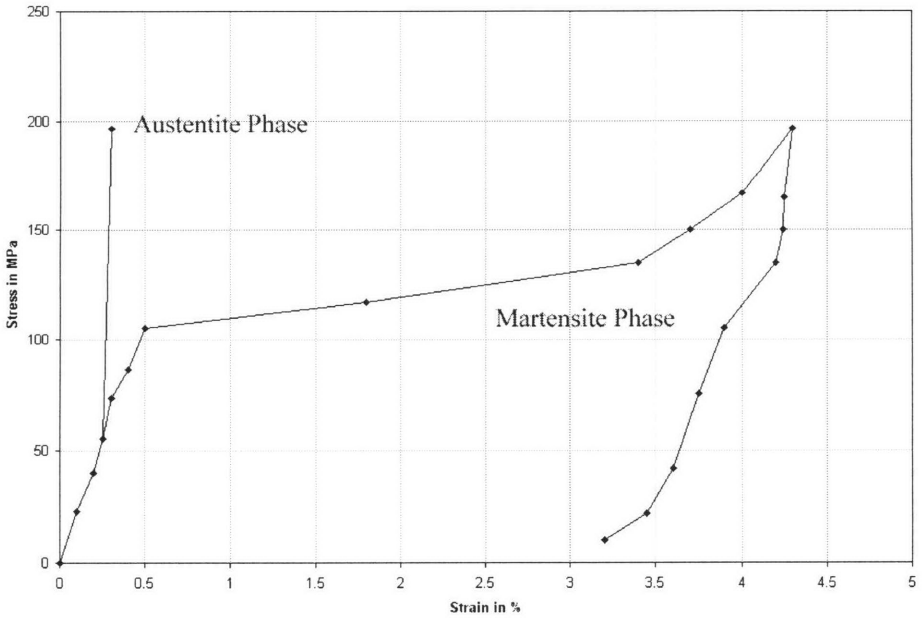

Figure 3.4: NiTi Stress-Strain Curve (Duerig, 1990)

There are some important design considerations in working with SMA's that can be very important. To avoid fatigue, the useful strain of an SMA should only be 3-5%, depending on the quality of the wire used. Also, there is a minimum bend radius for an SMA wire, depending on its diameter. Using a tighter radius will cause excess strain and failure in the wire.

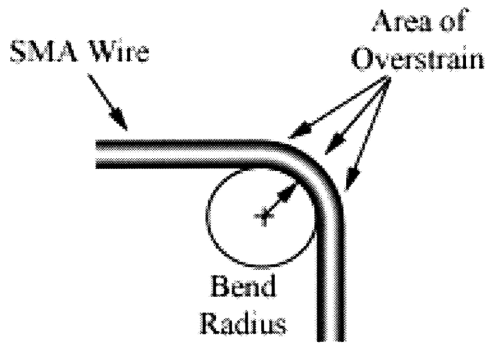

Figure 3.5: Large Bend Radius Causes Overstrain (Gilbertson, 1994)

Fixing the wire at each end is another design consideration. A thin wire has little surface area to clamp, yet exerts high force. Therefore, the clamp must hold enough of the wire to keep it from slipping. Soldering to a NiTi wire is difficult, because the heat associated with soldering can change the wire's properties. When using multiple wires in parallel, to increase force, each wire must be the same length, requiring special care in designing an SMA mechanism. If one wire is shorter than the others, it will bear all of the load when heated and break. Finally, care must be taken in the design of an SMA mechanism, to insulate the SMA wire. An electrical short across the SMA wire will make it useless.

3.4 Experimental Design

3.4.1 Goals

The goal of this reconfigurability work is to develop a shape memory alloy actuated mechanism to allow the rover to change geometry. Many concepts for changing rover geometry were looked at and evaluated. A mechanism that would simply change the rocker or bogie angle appeared to be more feasible with SMA's to implement than one that would actually extend or retract rocker or bogie links. Before choosing a design to be implemented on the rover, an initial test mechanism was developed to evaluate SMA performance and to learn more about implementation of shape memory alloys. The goals of initial work, therefore, are to use shape memory alloys to raise and squat a device similar to a rocker or bogie, and to test control of this mechanism's angle.

3.4.2 Force and Strain Requirements

Table 3.1 gives the requirements chosen for the reconfigurability mechanism. Since shape memory alloys only have a small useful strain, they must be attached close to the pivot point of a lever, to give that lever a useful range of motion. However, as the wires are moved closer to the pivot point, more wires will be required to achieve the necessary force. One way to "assist" the wires in lifting heavy load, is by using a bias spring to help offset some of the required force.

Several different configurations of springs and wires allow the mechanism to raise and squat, while loaded or unloaded (Figure 3.6). Configuration 1 simply uses SMA wires to raise the mechanism. Configuration 2 uses a spring that keeps the mechanism in a raised position. Wires above the pivot point allow the mechanism to squat when

actuated. However, both of these configurations require many and/or thick wires to achieve enough force to either lift the weight or stretch the spring. Using many wires adds complexity to the system. Using thick wires requires a larger bending radius. Both require more power to actuate.

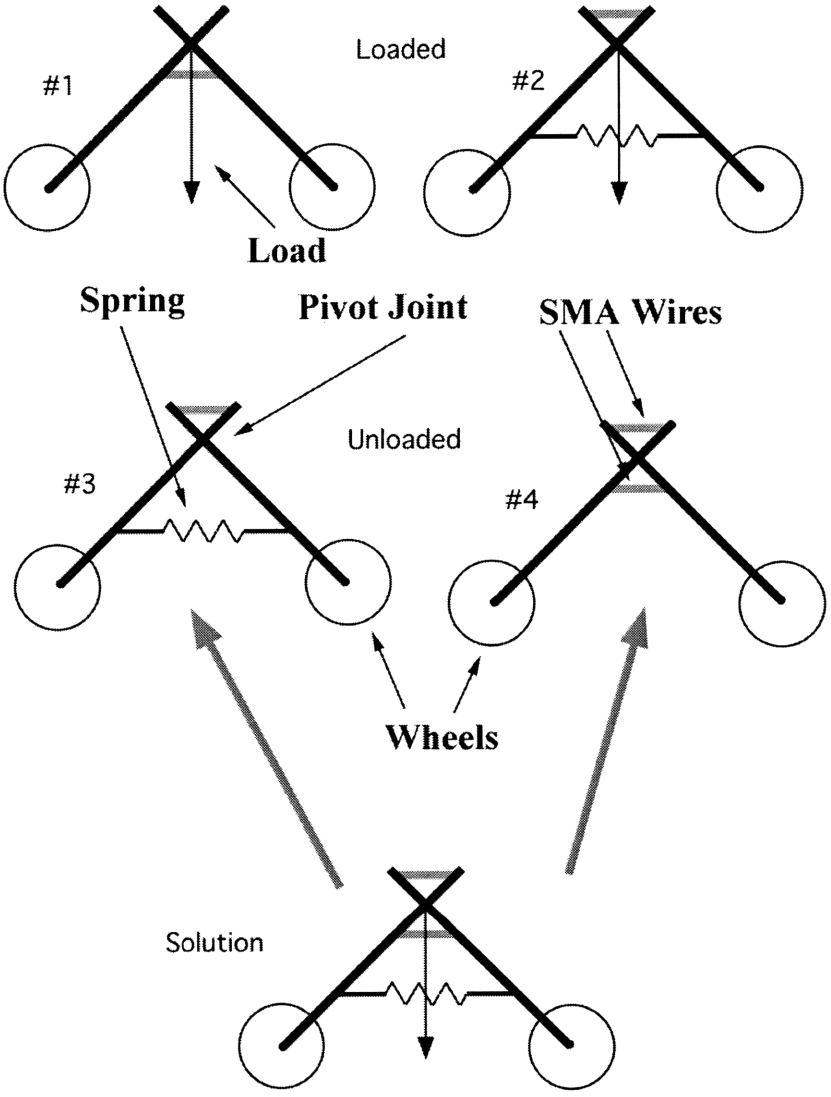

Figure 3.6: SMA and Spring Configurations

An unloaded mechanism would use different configurations of wires and springs. Configuration 3, because it is unloaded, uses a spring that is only stiff enough to stretch the SMA wire when not actuated. Since SMA's have a high ratio of actuated stress to

passive deformation stress, the unloaded system will use less power. Configuration 4 shows two sets of SMA wires. One set raises the system and one set squats.

The solution for the preliminary design is a combination of 3 and 4. In order to make the system behave like an unloaded system, a spring is be added with the correct stiffness to offset the payload weight. Then two sets of wires are used, one to raise and one to squat. The system can then be modified to test an unloaded condition, by removing the payload and using only the squat wires and the spring, as shown in number 3. Position control work using only one set of wires is simpler, and therefore a better starting place.

3.4.3 SMA Calculations

To implement the above design, several parameters would need to be determined: length and number of wires, distance from wires to pivot, wire diameter, and spring force. The useful length of wire deformation follows the strain equation,

$$\Delta L = L\varepsilon_{\max-useful} \tag{3.1}$$

where L is the length of the wire. The minimum force required to achieve this deformation is calculated using equation (3.2),

$$F_{deformation} = \frac{\pi n \sigma_{def} d^2}{4} \tag{3.2}$$

where n is the number of wires and d is the wire diameter. The maximum contraction force can be calculated using equation (3.2) by substituting the max. contraction stress for

the deformation stress. Finally the resistance, R, of the set of wires is obtained using equation (3.3),

$$R = \frac{4L\mathscr{R}}{\pi n d^2} \tag{3.3}$$

where $\mathscr{R}$ is the resistivity of the wire in Ohm*m.

Preliminary calculations showed that to use a reasonable amount of power and number of wires, the wire length would have to be an order of magnitude higher than the approximate wire length in Figure 3.6. The approach taken was to run the wires from one wheel, over or under the pivot, and back down to the other wheel (Figure 3.7). Rollers near the pivot point allow the full length of the wire to stretch and contract. This idea has the same effect as the one shown in Figure 3.6, but it allows for much higher strains due to longer wires.

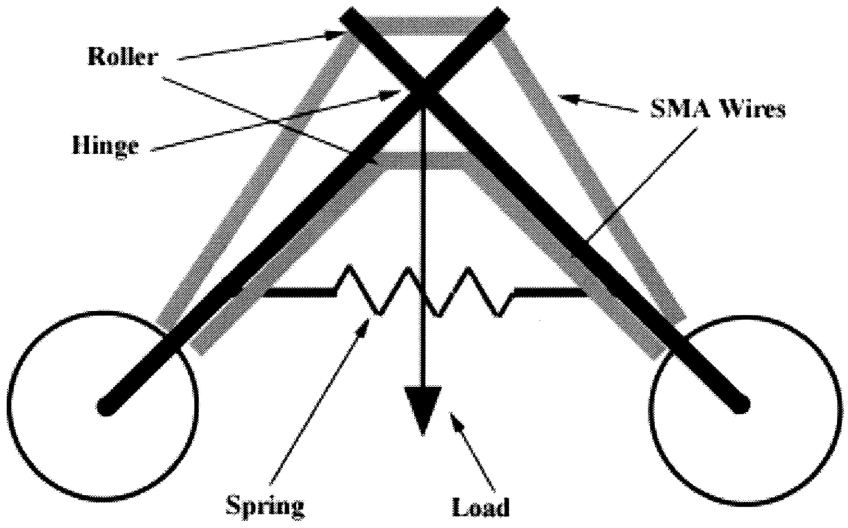

Figure 3.7: Longer Wires Design

Spring force is another concern. A standard extension spring follows the rule F=Kx. However, since the payload weight provides a constant force, an extension spring would provide excessive force at full extension and adequate or inadequate force in its retracted position. To simplify the model and reduce the work required by the SMA's at full spring extension, a constant force spring would be incorporated into the design.

3.4.4 Design Implementation

Figure 3.8 shows a schematic of the reconfigurability design, with a photograph of the mechanism in Figure 3.9. The same size aluminum tubes as used in the rover, were used as the structure of this device. The rollers are grooved aluminum cylinders. To insulate the wires, the aluminum rollers use Phenolic shafts (a polymer based composite) instead of tradition steel shafts. The wires are friction clamped at each end using fiberglass plates, again for insulation. The constant force spring is wrapped around an aluminum drum that is free to rotate. A potentiometer mounted at the pivot point measures the angle of the mechanism.

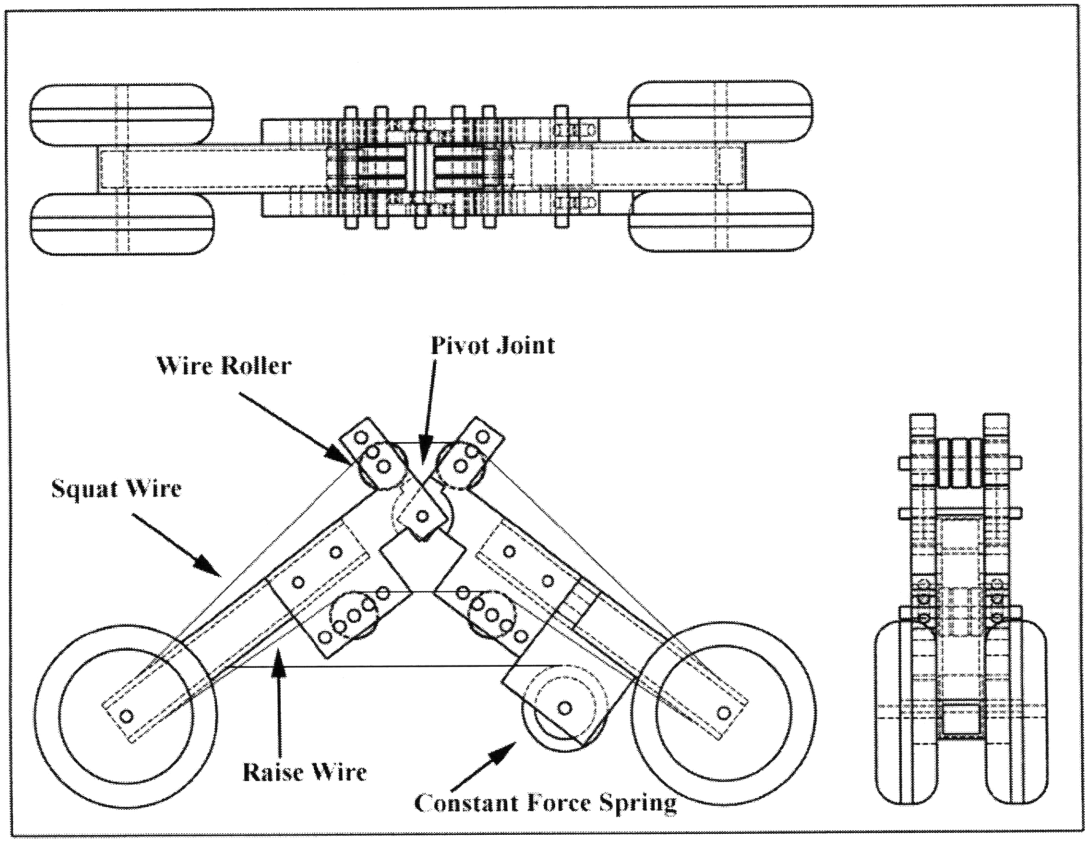

Figure 3.8: Mechanism Schematic

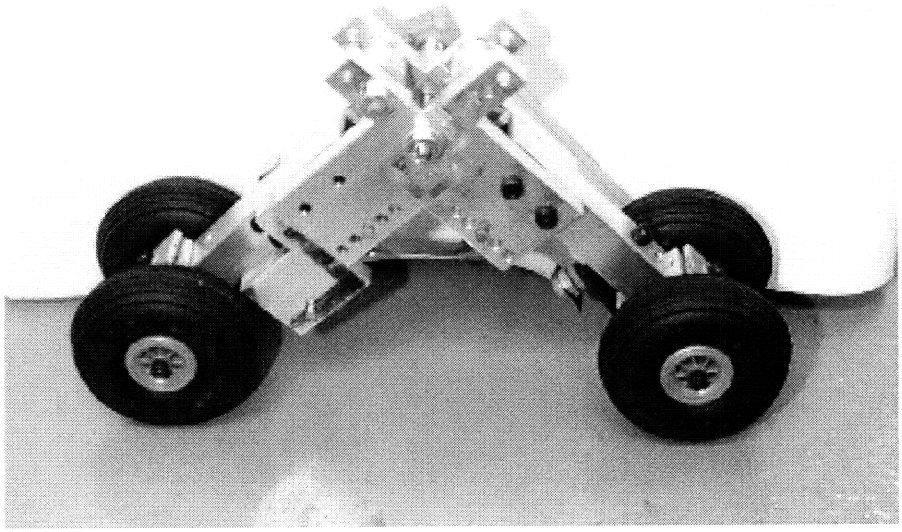

Figure 3.9: Mechanism Prototype

3.5 Experimental Results

3.5.1 Bipolar Position

The system was first tested in a loaded configuration (Figure 3.6: Solution). Without the SMA wires, the system was stable in either the fully raised or fully squatted position, as predicted. Upon actuation of the wires, the mechanism raised and squatted with rise times on the order of ½ second for the full 60° of motion.

3.5.2 Position Control

Position control experiments were performed with the reconfigurability configuration shown below (Figure 3.10). The one pound payload was removed and the lower (raise) wires were not used. This is the simpler of the two configurations to control, and therefore a better starting point. A proportional position control loop was written in C++, and position measurements were read from a potentiometer mounted to the joint. The high current needs of the SMA's were met by a custom built transistor circuit (Troisfontaine, 1998).

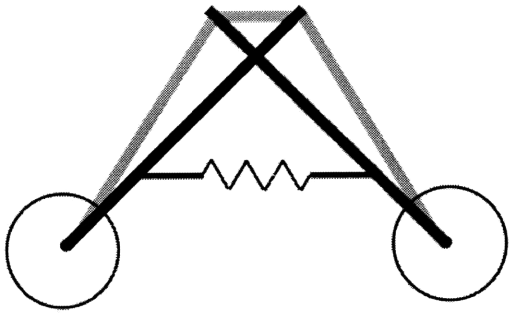

Figure 3.10: Position Control Configuration

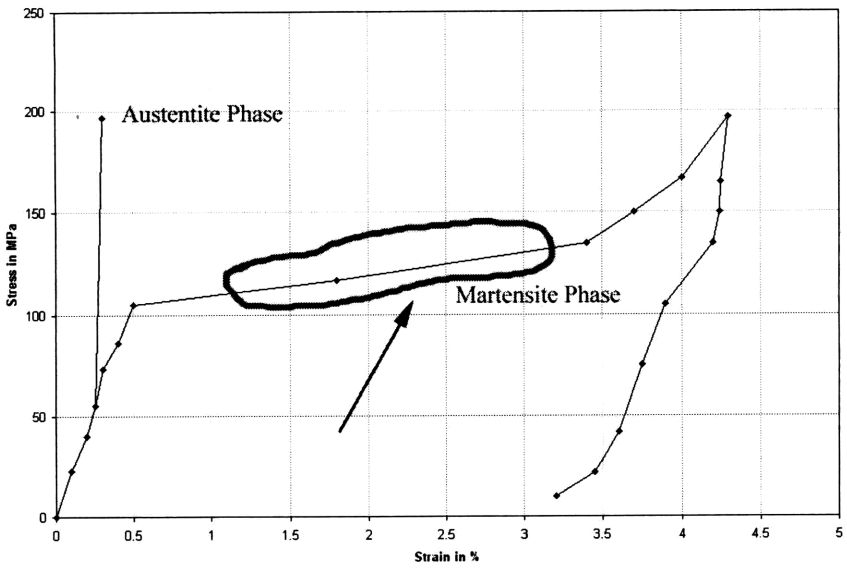

Figure 3.11: Transition Phase

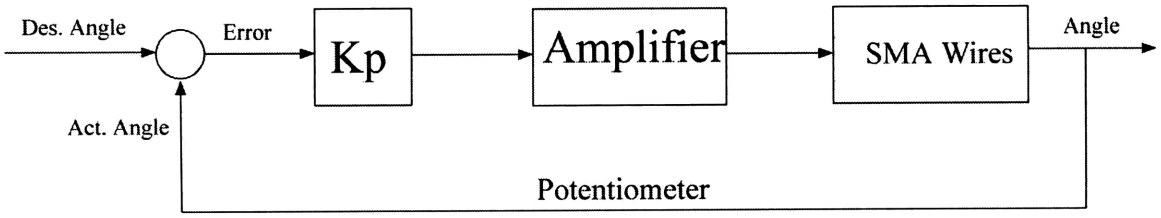

Figure 3.12: Position Control Block Diagram

The first task was to determine the holding current. This is the current required to keep the SMA between the austentite and martensite phases, as illustrated in Figure 3.11. This current would be the current sent from the amplifier when the position error (desired position – actual position) was 0. Then the proportional gain, Kp, was tuned to optimize performance. Figures 3.13-3.15 presents test results for three different desired angles. The peak power used was 1.9 Watts.

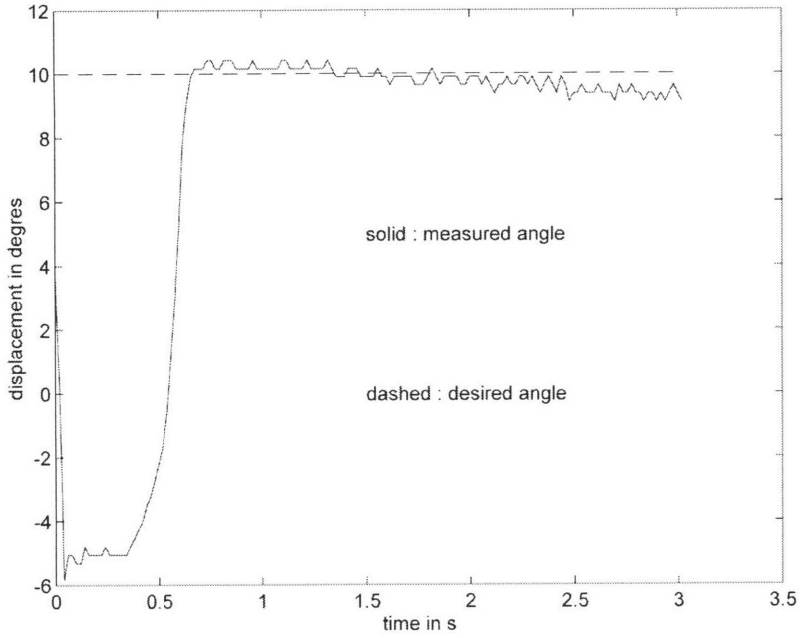

Figure 3.13: 10° Step

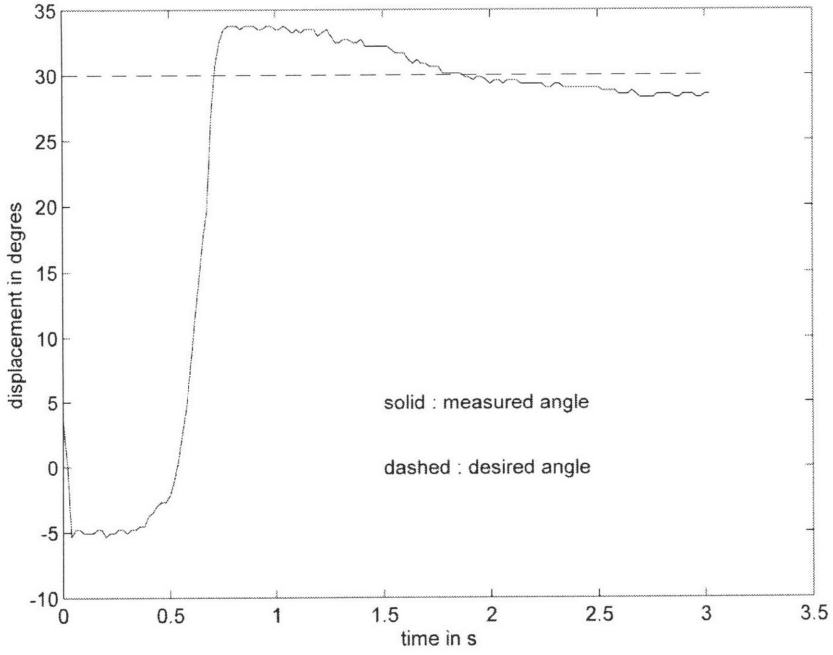

Figure 3.14: 30° Step

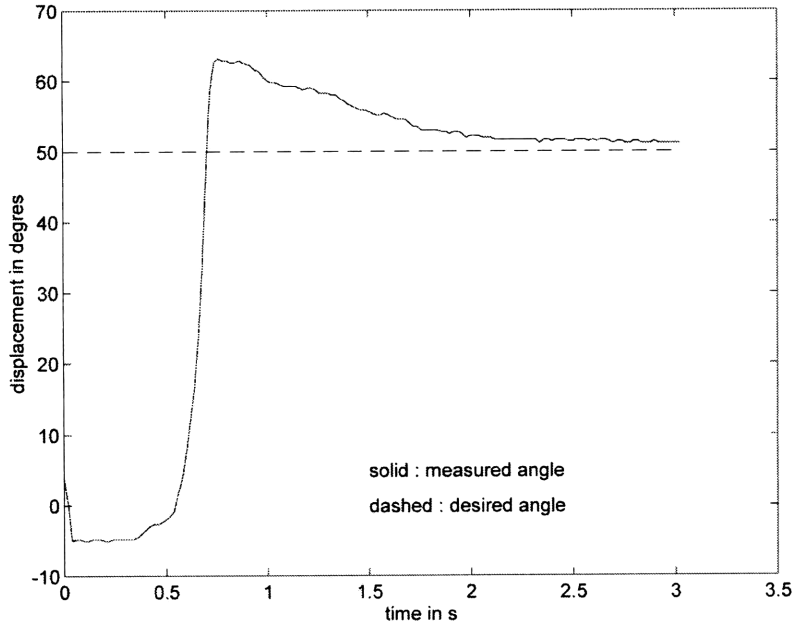

Figure 3.15: 50° Step

3.5.3 Analysis

These plots show a rather typical P control response. Due to low damping, there is some overshoot in the two larger steps. Also there is some steady state error. If position accuracy better than a few degrees is required, than an integrator term would be necessary. Another observation is the one-half second lag before the mechanism begins to move. This lag is due to a "cold start" by the system. The current being sent to the wires was zero, not the holding current, when the test began. Therefore, the lag is the time it took for the wires to heat up from room temperature. One key observation that is not shown in Figures 3.13-3.15 is that this system exhibits very poor disturbance rejection, typical of P control. Using higher gains, however, cause the system to oscillate. PID control may solve this problem as well as the steady state error problem.

Many design improvements will need to be made, however, before this system can be incorporated into the rover. First, the wires may have slipped in the friction clamps. Thie issue will need further investigation and possibly a better method of fixing the wires will be necessary. Also, this test system uses free rolling wheels, where as the wheels may not be free to move on the rover if it is stuck. Also, as mentioned earlier, the position control tests above were done with the system unloaded. Further tests will have to be performed with different payloads and possibly using both sets of wires and a more robust control scheme. Power considerations dictate that this system cannot be actively running all of the time. To keep power usage down, control should only be done for one or two seconds at a time, just enough time to achieve the desired position. The two sets of wire acting against each other will both be in the stress-strain curve location shown in Figure 3.11. Therefore, small outside force will cause the mechanism to change angle. One solution to this problem is to incorporate a brake that passively locks the system in place. When a new angle is desired, the brake is released momentarily by another SMA wire, and the angle can be changed. Then the brake is released and the system locks. Thus only a few seconds of power would be used. The next section presents a new design based on these results.

3.6 Second Generation Design

The new design for rover reconfigurability is shown in Figure 3.16. Illustrated is the rocker of the rover's left side. One key feature is the Delrin© wire guides, which replace the aluminum rollers. Delrin gives the wires a low friction, insulated surface to slide on. The guides also protect the wires, which were exposed in the first generation design. The second key feature is the addition of a brake. A multi-jaw coupling locks

the rocker links in place, fixing the angle. The jaws are held together by a compression spring located underneath the other side of the brake pivot lever. An SMA wire is hidden inside the aluminum tube next to the spring. When the SMA wire is heated, it pulls the brake pivot lever towards the tube, opening the jaws and allowing the other SMA wires to change the rocker angle.

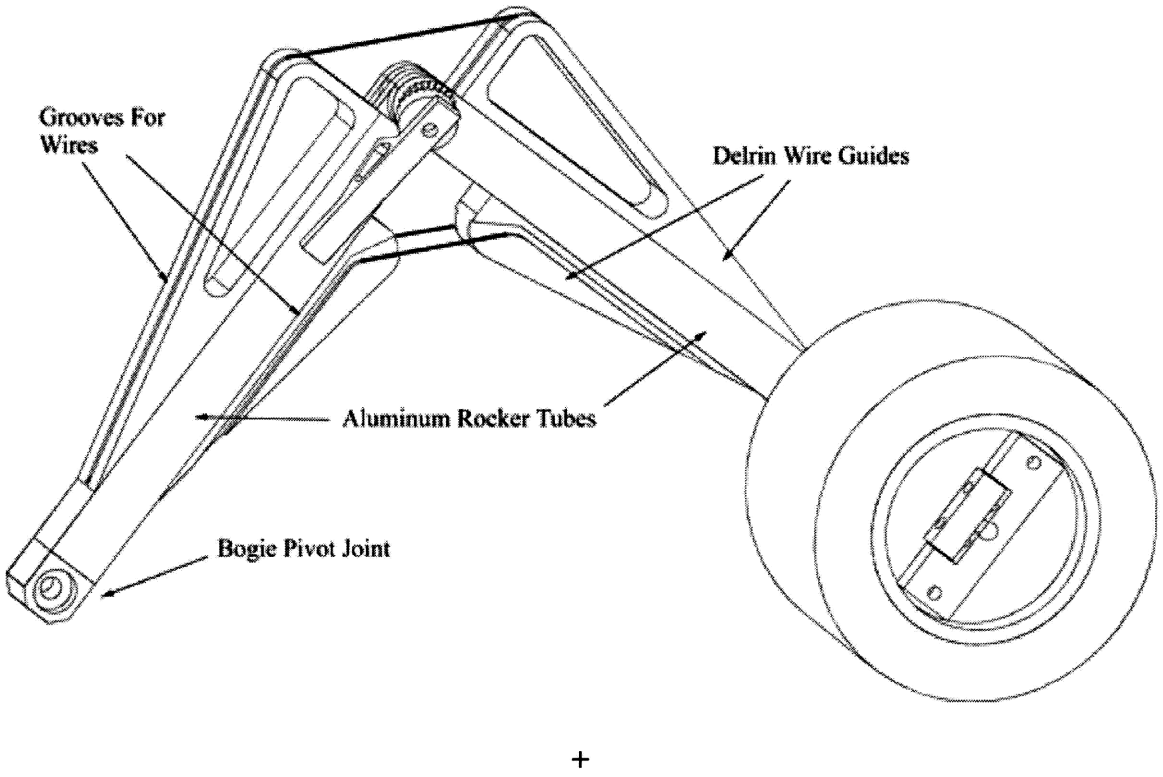

Figure 3.16: Second Generation Design

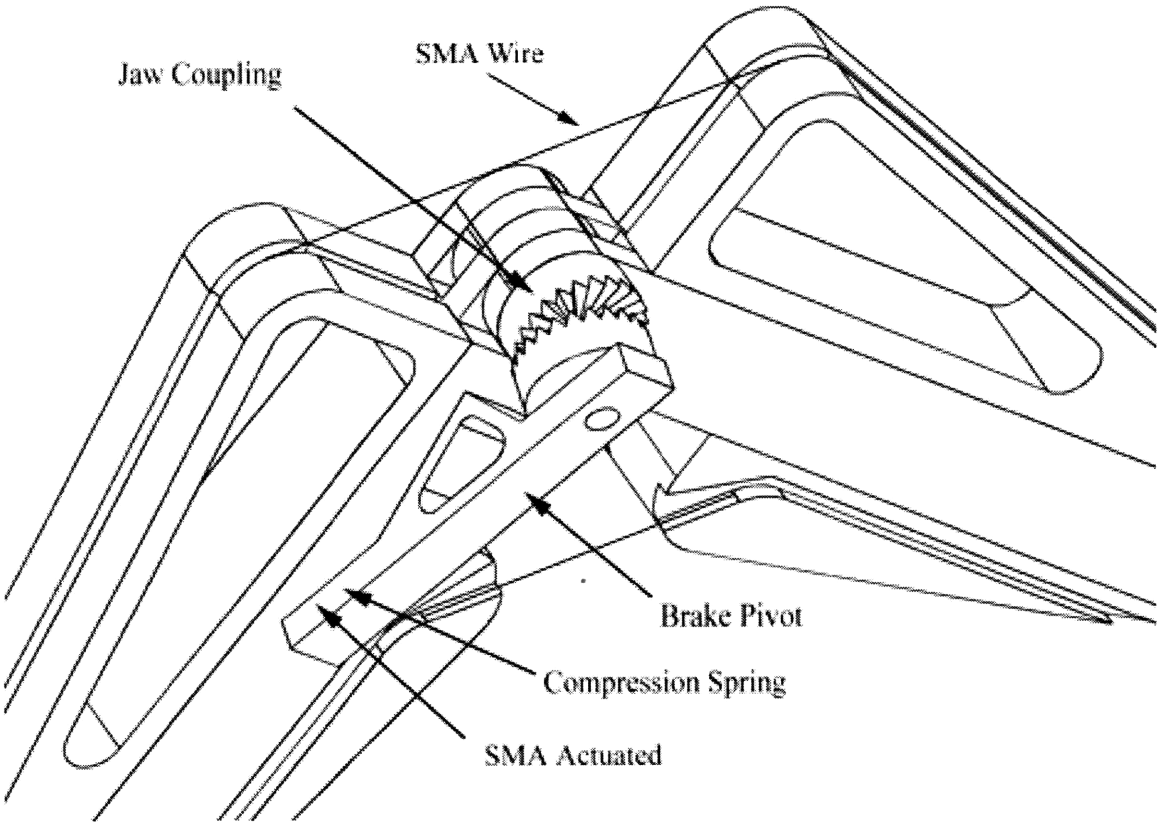

Figure 3.17: Brake Close-up

4 Manipulator

4.1 Introduction

The next addition to the planetary rover experimental system is a manipulator and end-effector. As with the rover, the manipulator is controlled and powered remotely through a tether. The manipulator is to serve as an experimental test bed for two areas of research. First, a method for the rover to improve its capability to traverse rugged terrain is to use its manipulator for assistance. For example, the rover can use the manipulator to shift its center of mass, thus achieving traction control in a different way than was discussed in chapter 3. Also, if the rover becomes trapped, and can not free itself even with traction control, then the manipulator can exert a force on the ground and free the rover from its entrapped position. The other focus of manipulator research is to develop friction compensating control of a manipulator from a compliant base using a six degree of freedom force torque sensor. This new control method, known as BSC control, uses the force-torque sensor at the base of a manipulator to estimate the torque at each of the arm's joints. Knowing these torques, the friction in the manipulator can be compensated for, and end point precision can be improved (Iagnemma *et al.*, 1997). The sensor also allows the manipulator to sense when it has come into contact with another object. This information can be useful when grasping rocks, or when drilling into or grinding a rock surface.

The next section outlines the manipulators that JPL is developing. Section 4.3 presents a preliminary and a final design for the manipulator. Section 4.4 discusses

predicted performance of the arm, and Section 4.5 compares these predictions with experimental data.

4.2 Background

JPL is developing a series of lightweight manipulators to be used on the '01-'05 missions. These manipulators will be mounted to the front of the rover and have a multi degree of freedom end-effector. The MicroArm-I and the MicroArm-II are 3 DOF anthropomorphic arms. They use 2D carbon fiber tubes for the links and a new 3D carbon fiber machineable composite matrix for the joints, to decrease weight. Ultrasonic motors (USM's) are also being incorporated due to their high torque/mass ratios. Due to power requirements, actuators must have a high torque/speed ratio, another attribute of USM's. Table 4.1 shows some data on JPL's rover mounted anthropomorphic arms (Shenker).

Table 4.1: JPL and MIT Arm Data (Schenker, *et al.*, 1997)

Arm Data	MicroArm-I	MicroArm-II	Mod 2
Length	.7 m	similar to MicroArm-I	.21 m
Weight	1 kg	?	.43 kg
Weight w/end effector	1.5 kg	1.9 kg	.48 kg
Material	3D Composite	3D Composite, high density	2024-T4 Aluminum
Actuation	UltraSonic Motors	DC Motors, PID	DC Motors, PID
Payload	>1x	2x	2x

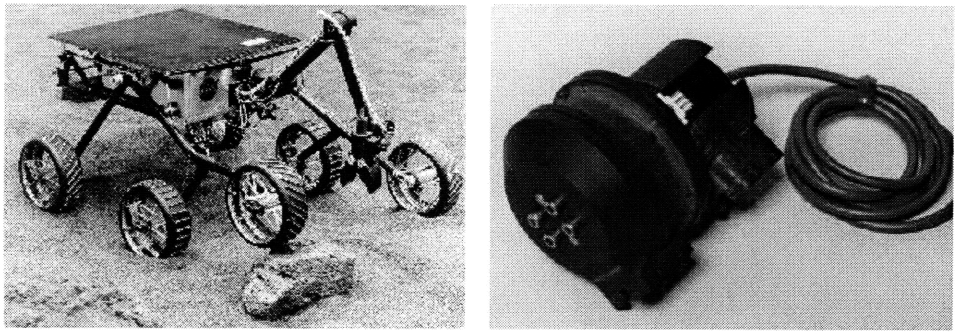

Figure 4.1: JPL's Micro Arm and USM Motor (Shenker, *et al.*, 1997)

4.3 Design

4.3.1 Functional Requirements

The functional requirements for the experimental manipulator are:

I. Three DOF Anthropomorphic

II. Exert one-half rover weight in bent position (4 lbs.)

III. Payload of 2 lbs at full extension

IV. Lightweight (<28 oz.)

V. Stiff (links an order of magnitude stiffer than gear heads)

VI. Reach ground (base is 5" above ground)

VII. Able to put rock on top of rover body (2 lb rock)

Requirement II allows the arm to help remove the rover from a trap, III allows sizable rocks to be manipulated, and VII allows for the storage of rock samples. Manipulator weight is largely dependent on actuator weight. Due to cost considerations,

DC motors with gear heads would be used. Aluminum links, if designed well, do not add substantial weight over carbon fiber, and are easier to machine.

The arm link lengths are determined based on workspace requirements. The arm must have a minimum length so that it can reach the ground. Different link lengths were simulated in Pro/ENGINEER to show what areas these lengths would allow the arm to access. An 8 inch arm length allowed access to a ground circle that was bounded by the two front tires. A 12 inch arm was necessary for the arm to reach to its side, over the two front wheels. However, this length only allowed for a small point of access on each side. A 16 inch manipulator would be required to have a useful manipulator workspace on either side. Due to weight and stiffness considerations, the 8 inch arm length was chosen.

The next section (4.3.2) presents a preliminary manipulator design. Several improvements to this design led to a substantially different final design. This final design, which is the one that was built and tested, is detailed in section 4.3.3.

4.3.2 Design 1

The preliminary manipulator design is shown in Figure 4.2. For volume considerations, the shoulder and elbow motors are housed along the joint axis. The selected motors are too long to simply attach to one side of the joint, because the motor, gear head, and encoder are in a series. To enable the joint to pivot, a thin aluminum case around the motor provides a seat for large diameter bearings. The aluminum case is fixed to one link by a split clamp. The other link is press fit over the bearing outer race, thus allowing rotation. The upper arm and forearm links are low weight ¼ inch aluminum plates. The fixed base of the arm is a gear which is then bolted to the 6 degree of freedom force-torque sensor. The torso of the arm rotates about the gear as a motor

mounted to the torso walks around the base gear. This arm meets all of the above requirements, however there some problems with the design.

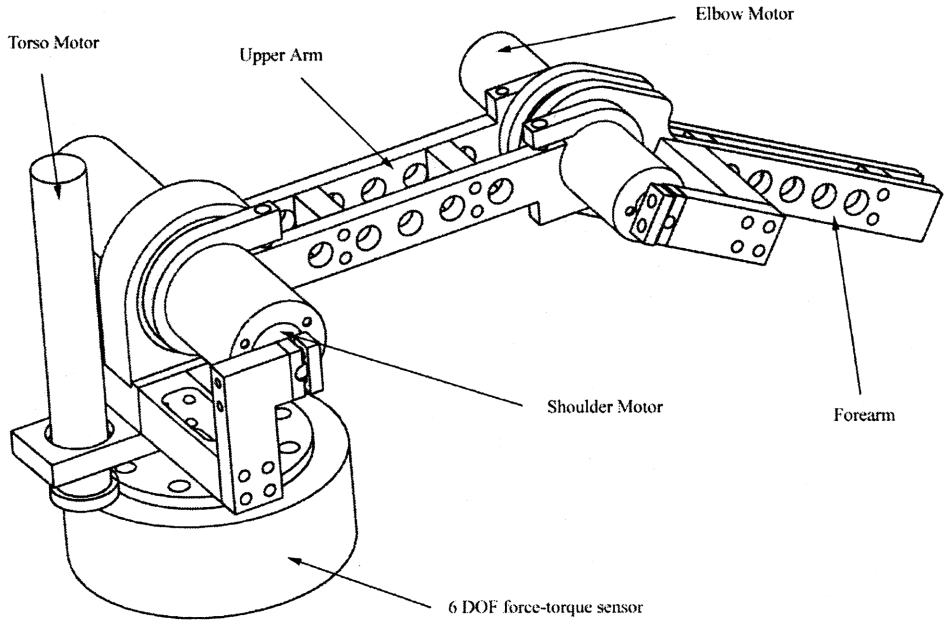

Figure 4.2: Preliminary Manipulator Design

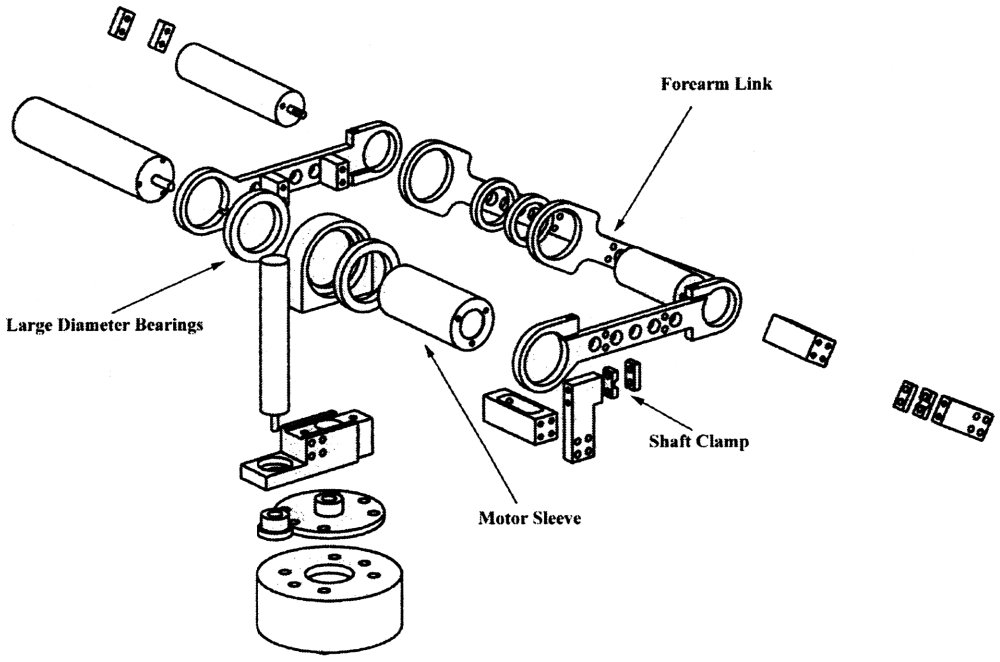

Figure 4.3: Preliminary Design Exploded View

The biggest design problem results from the elbow and shoulder motors being mounted along the joint axes. Because those two gear head shafts are rigidly clamped to the arm links, there are effectively four bearings in a line. Aligning the gear heads with the large diameter bearings would be extremely difficult because several parts are bolted in a series between the shaft and the link.

There is also room for improvement in both manipulator weight and complexity. As mentioned before, the motor/gear head combinations make up a substantial amount of the arm's weight. Gear head miniaturization is limited by the output torque required. Therefore, a smaller gear head would require additional external gearing. The required output torque for the shoulder gear head can also be reduced by moving the elbow motor closer to the shoulder axis. This reduces the moment caused by the weight of the elbow motor and gear head on the shoulder gear head. Another contribution to high manipulator weight is the links. These links are ¼" aluminum plates that have a simple rectangular cross-section. A stiffer, lighter link could be designed using a thin walled I-beam or tube section.

4.3.3 Design 2

4.3.3.1 *Overview*

Solutions to the problems associated with Design 1 were incorporated into a new design (Design 2) shown in Figures 4.4 and 4.5. There are three features which distinguish this design from the previous one. First, the shoulder and elbow motors have been moved away from the joint axes. They are geared down between the gear head and the joint, thus allowing for smaller and lighter motors and gear heads. The second

improvement is that the upper arm and forearm links have been changed to thin walled, high stiffness sections. Finally, this design is less complex in that there are fewer parts that must be machined. Sections 4.3.3.2, 4.3.3.3, and 4.3.3.4 discuss each manipulator joint in detail.

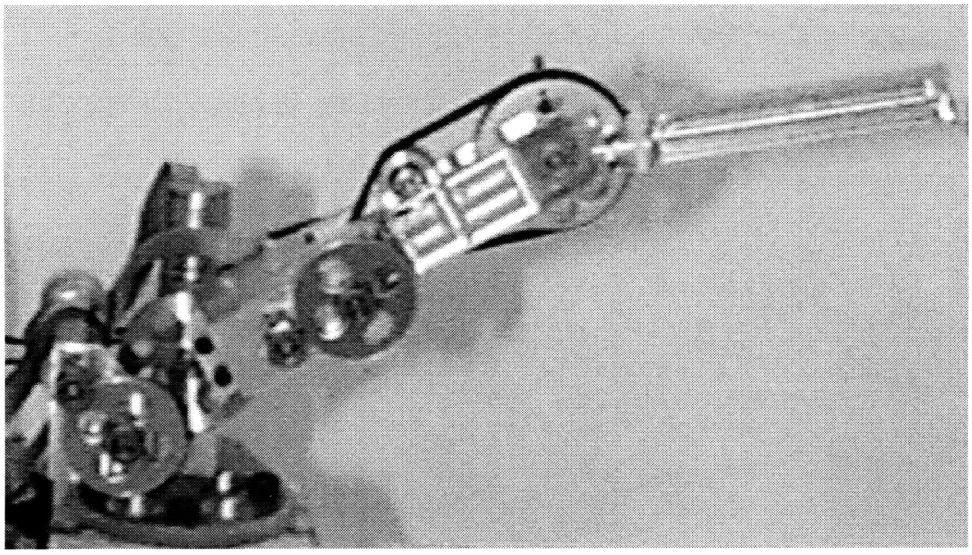

Figure 4.4: Manipulator Prototype

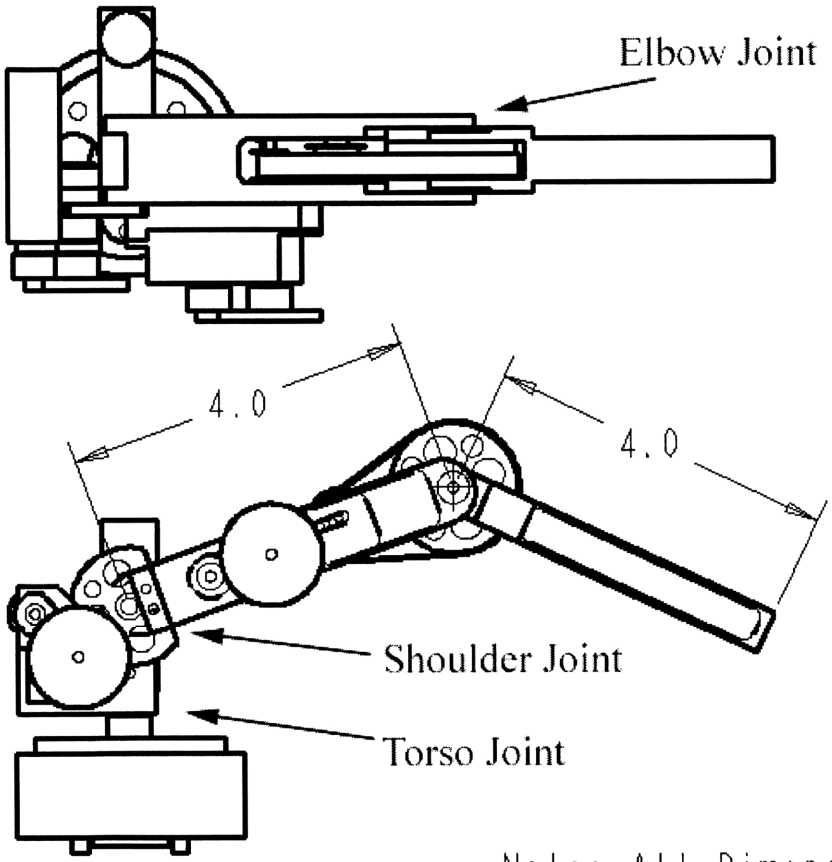

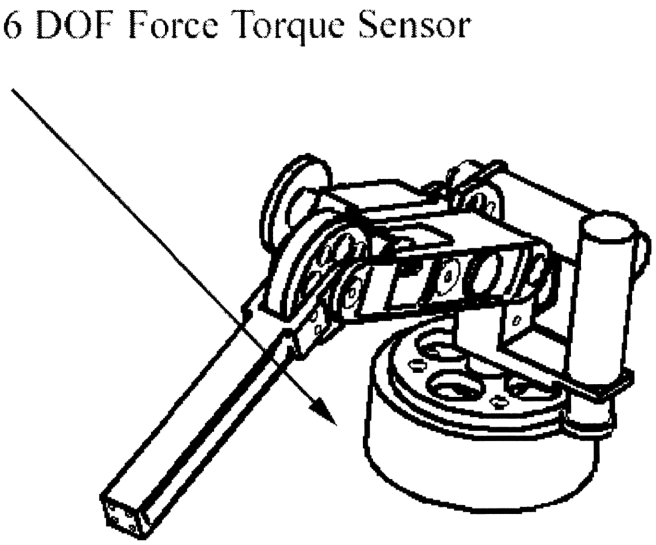

Note: All Dimensions in Inches

Figure 4.5: Manipulator Schematic

4.3.3.2 *Torso*

The torso joint is very similar to the torso joint in Design 1. Again, the base of the manipulator is an aluminum gear which is bolted to the force-torque sensor. Holes were placed in the gear to lighten it. Figure 4.6 shows a cross-section of the manipulator's torso. The pivot shaft is slip fit into the base gear, and held in axially by a soft tipped set screw. A thin walled spacer separates the two bearings, and an E-clip on the pivot shaft holds the bearings on the shaft. A set screw axially holds the spacer to the torso block. A 3 to 1 ratio of bearing spacing to bearing inner race diameter was chosen. As in design 1, the torso motor is bolted to the rotating torso block and walks around the fixed base gear. With conventional gears, backlash would cause repeatability problems. Therefore, an anti-backlash gear head was used in conjunction with the motor.

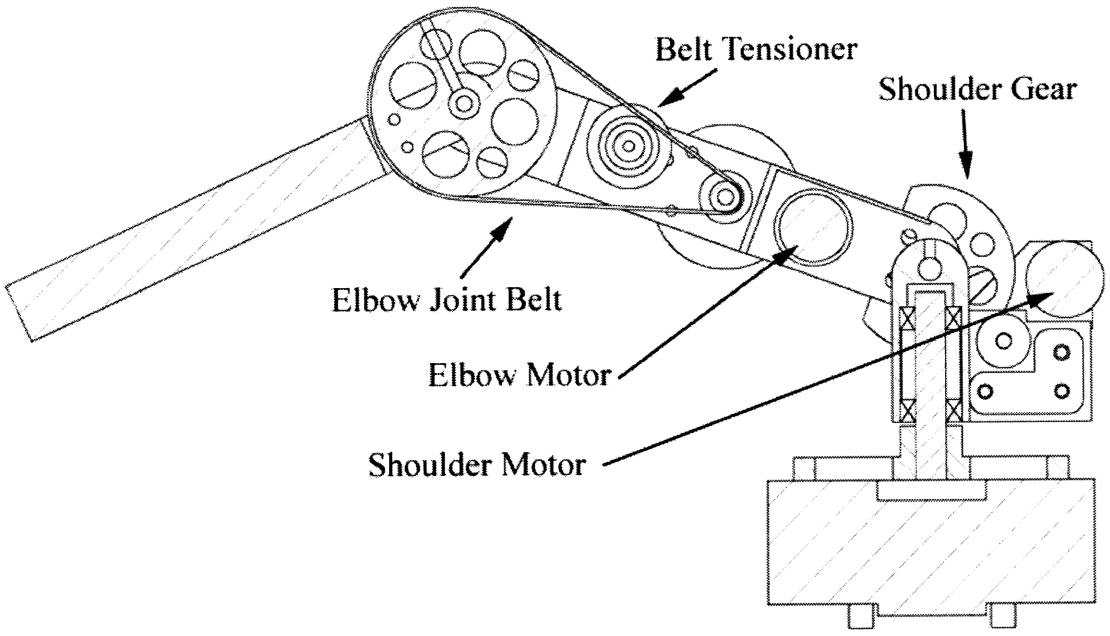

Figure 4.6: Manipulator Cross-section

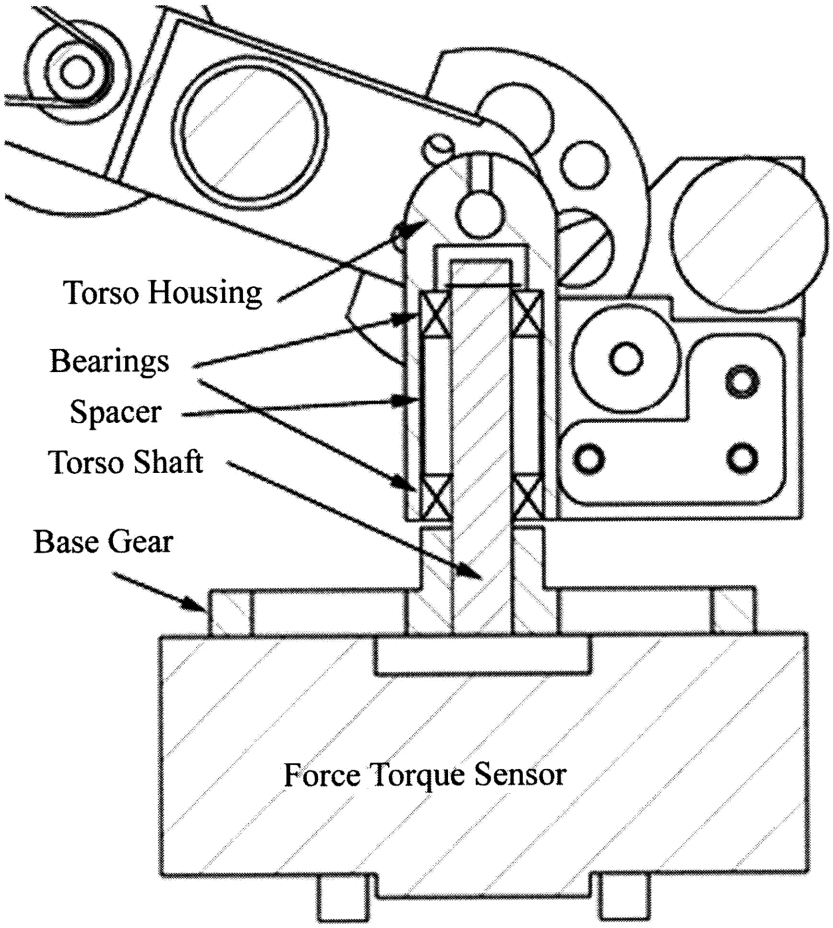

Figure 4.7: Torso Joint Cross-section

In addition, an anti-backlash pinion is used to walk around the base gear. The anti-backlash pinion is essentially two gears, back to back, which rotate relative to each other. This rotation is spring loaded, so that the two gear halves close any gap between them and the other gear. However, when the arm was assembled and tested, the spring inside the anti-backlash gear was not stiff enough to overcome bearing friction and move the arm. Therefore, the anti-backlash gear was modified, as shown in Figures 4.8 and 4.9. An inserted piece of metal effectively shortened the length of the spring beam, stiffening the spring substantially.

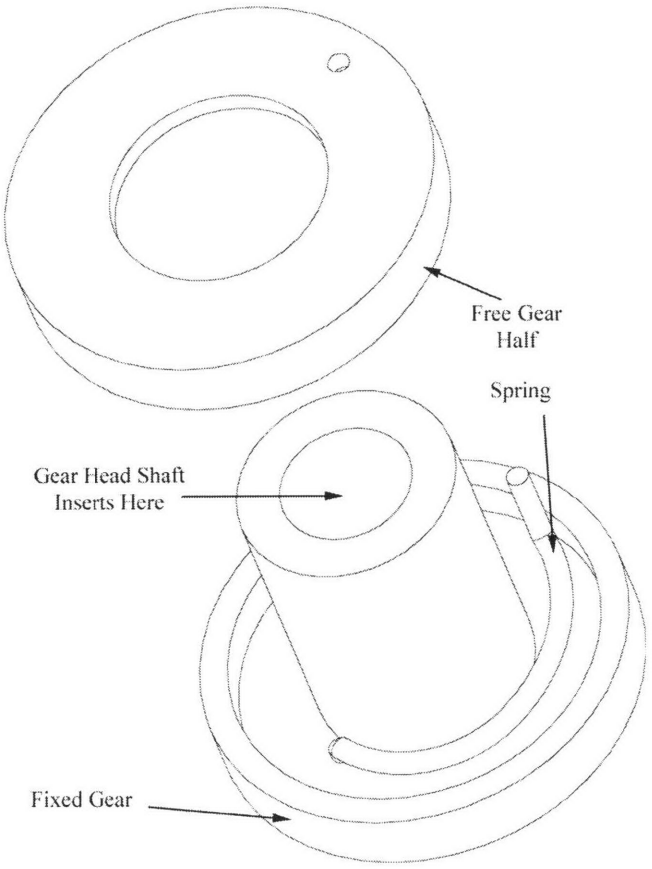

Figure 4.8: Anti-Backlash Gear Exploded View

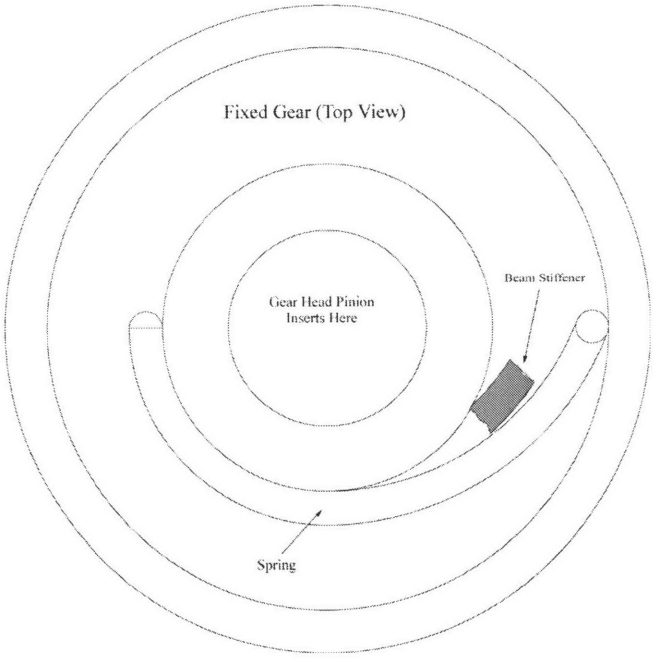

Figure 4.9: Anti-Backlash Gear Stiffener

4.3.3.3 *Shoulder*

The shoulder motor has been moved behind the shoulder joint axis. This allows for the gear head to be geared down further, resulting in a smaller motor and gear head. The motors, gear heads, and encoders used for the manipulator are listed in Appendix B. The gearing for the shoulder joint is a two stage assembly, providing a 3093:1 ratio, in addition to the 134:1 ratio of the gear head. The two bearings of the intermediate gear shaft are pressed into two different parts. This was done so that the shaft can be aligned for perfect gear mesh by adjusting the fit between the two parts.

4.3.3.4 *Elbow*

The elbow motor was also moved off the joint axis. However, to reduce the moment that the motor puts on the shoulder joint, it has been moved as far from the elbow joint as possible. Therefore, a belt is required to transmit torque from the motor to the joint. Two 3/16" timing belts were used due to their stiffness and ability to be used with very small diameter pulleys for high gear ratios. Two belts were used because a 3/8" belt was not available, and this width is the minimum required to lift the 2 lbs payload, based on the manufacturer's recommendations. To keep the belt tight, an adjustable tensioning pulley was added to the design.

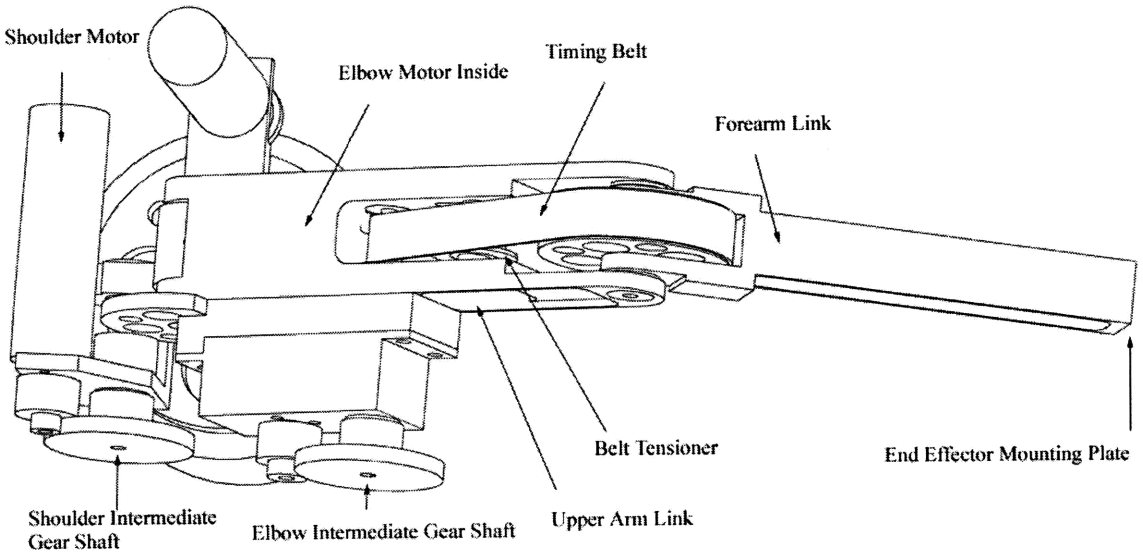

Figure 4.10: Shoulder and Elbow Joints

The upper arm link is machined out of a solid 1"x1"x4" block of 2024-T4 aluminum. Many of the surfaces are machined to 30 thousandths of an inch thick to keep weight down. The forearm link has 30 thousandths walls as well, and has an I-beam cross section. This link has a square mounting plate on the end for different end-effectors to be bolted to. Schematics of the two links are shown in Appendix C.

4.4 Analysis

4.4.1 Precision

Backlash in the torso joint is eliminated with the anti-backlash gear. For most applications, the elbow and shoulder joints will be gravity loaded in the same direction, eliminating gear backlash as well. Therefore, joint position repeatability should be at the level of encoder resolution. The encoders used for the manipulator are 16 pulse per revolution magnetic encoders. They have two channels, out of phase by 90°. With

quadrature logic, the encoder boards can resolve 64 counts per revolution. Thus the resolution in joint radians can be calculated using equation 4.1 below,

$$E = \frac{2\pi}{64 R_{gh} R_{eg}} \tag{4.1}$$

where E is the joint resolution in radians, R_{gh} is the gear head ratio and R_{eg} is the external gear ratio. Table 4.2 shows Equation (4.1) calculated for the three manipulator joints. The errors listed represent the theoretical precision of the system, assuming optimal control so that actual resolution is to within one encoder count.

Table 4.2: Theoretical Precision

Joint	Gearhead Ratio	External Gear Ratio	Final Gear Ratio	Pred. Error (μrad)
Elbow	133.5	22.2	2961.7	33.1
Shoulde	133.5	23.2	3092.6	31.7
Torso	261.4	3.6	944.0	104.0

The accuracy of the manipulator depends on the deflection of various parts caused by external forces. These external forces can be gravity, wind, or contact with an object. Table 4.3 lists the various elements that can cause significant deflection in the manipulator. The stiffness of the timing belt could not be obtained from the manufacturer, and therefore remains an unknown. Gear head deflection is unknown and will have to be determined experimentally. Bending deflection of both the upper arm and forearm links appears to be negligible compared to the torsion of the intermediate gear shafts. The actual bending stiffness of the upper arm would have to be determined using FEA, as it does not have a uniform section with which to calculate the cross-sectional moment of inertia. A rough estimation gives a stiffness of five times that of the forearm link.

Table 4.3: Deflection Calculations and Results

Element	Deflection	Pred. Stiffness Nm/rad	Exp. Stiffness Nm/rad
Forearm Link	Bending	833.5	
Belt	Tension	not available	
Intermediate Gear Shaft	Torsion	94.6	
Gearhead	Torsion	not available	115.3
TOTAL		?	22.4
Upper Arm	Bending	~5x Forearm Stiffness	
Intermediate Gear Shaft	Torsion	203.8	
Gearhead	Torsion	not available	115.3
Torso Shaft	Bending	821	
TOTAL		?	113.6

4.5 Experimental Results

4.5.1 Response

The manipulator is operated using PID control and three current controlled amplifiers. Figures 4.11-4.13 show the response of the three manipulator joints to a 45° step input. The elbow and shoulder joints show rise times of 0.3 seconds, while the torso joint is much faster at 0.15 seconds. The elbow joint has a 17% overshoot, the shoulder joint 14%, and the torso joint has a large overshoot of 88%. Both the elbow and shoulder joints exhibit performance typical of PID. The torso joint has some problems with steady state error. As seen in the plot, it tends to "hunt" back and forth across the desired position. This poor performance is due to high friction in the system, normally attributed to the anti-backlash gear where friction is considerably higher. Also, at the time this data was gathered, there appeared to be some damage to the gear head. A crash of the system may have caused the gear head to become partially stripped. Before the crash, performance was better, but hunting was still observed.

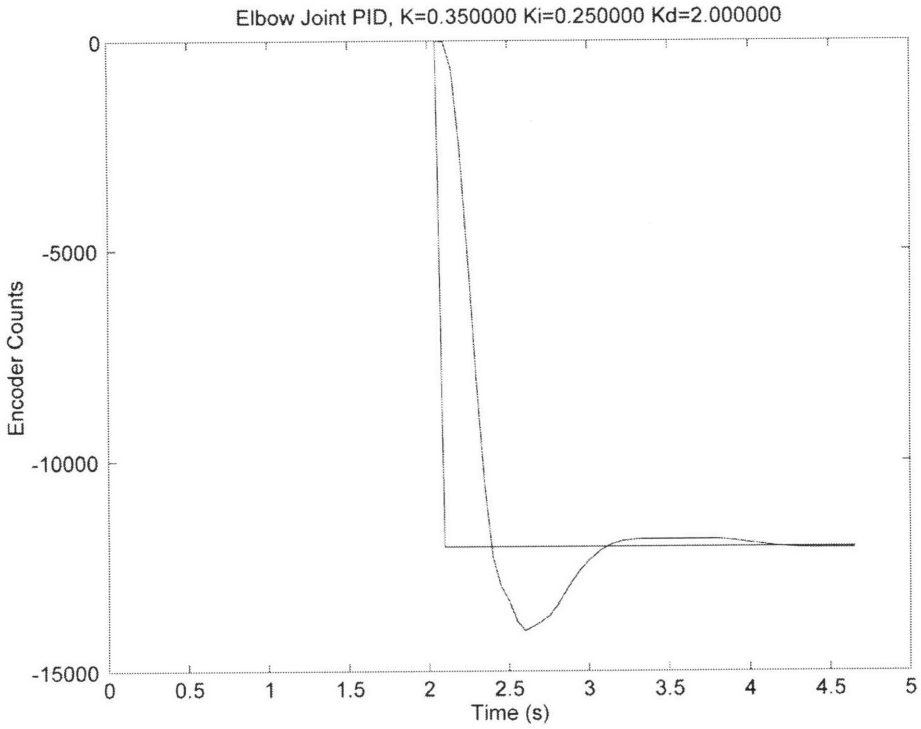

Figure 4.11: Elbow Joint Response

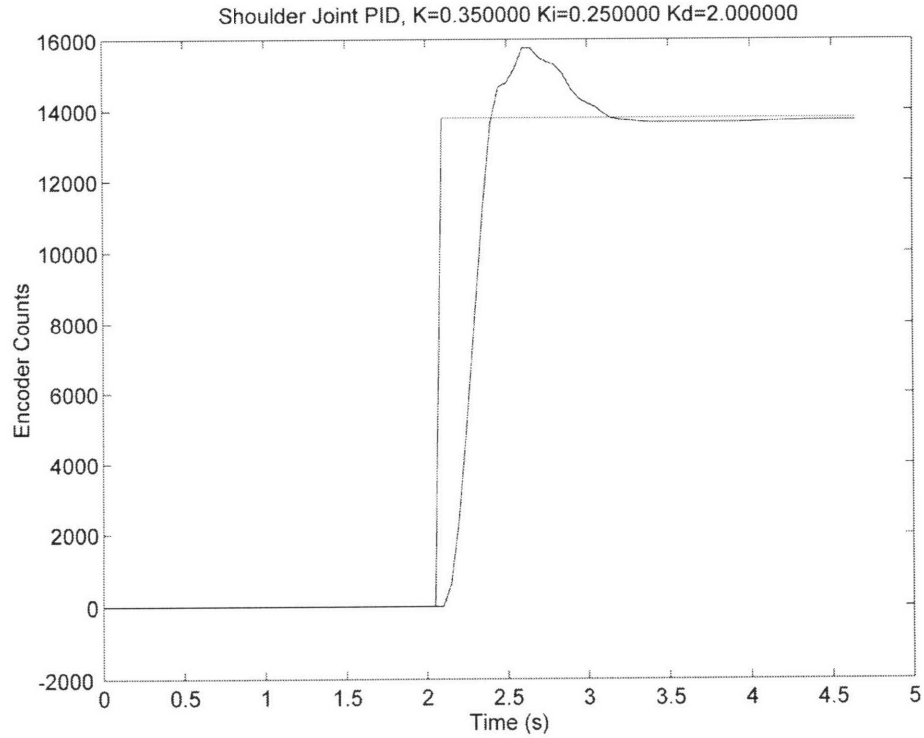

Figure 4.12: Shoulder Joint Response

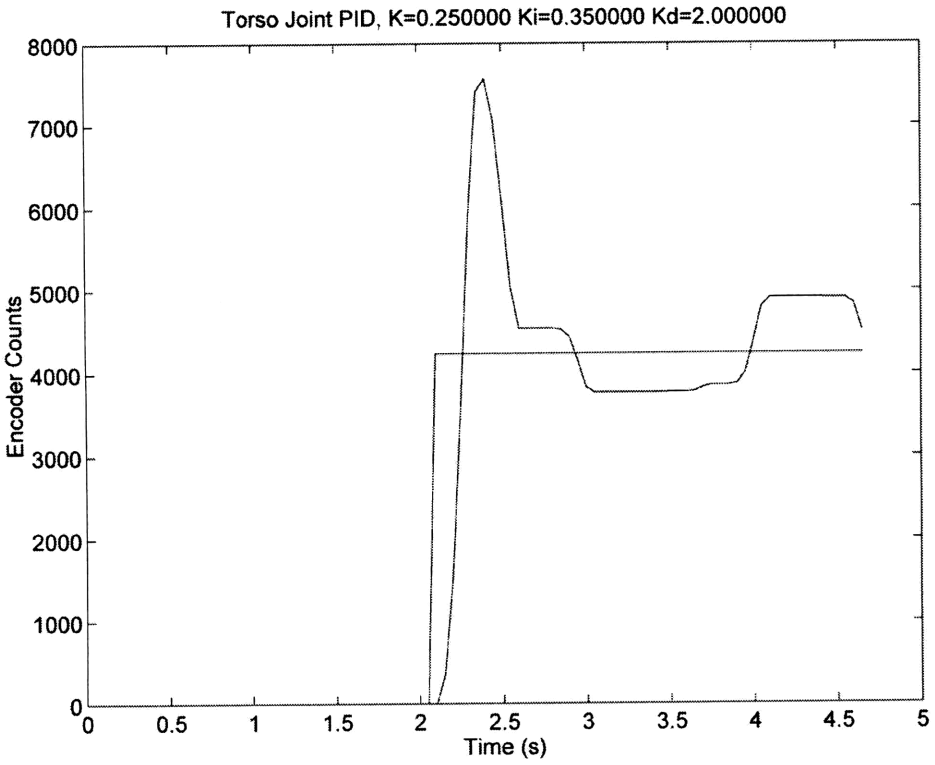

Figure 4.13: Torso Joint Response

4.5.2 Repeatability

Steady state error in the manipulator system separates ideal and actual repeatability. While ideal repeatability is one encoder count (33, 32 and 104 μradians for the elbow, shoulder and torso joints respectively), experimental repeatability was higher. Repeated tests on the elbow and shoulder joints gave steady state error over both 5 and 10 second intervals. Average repeatability errors were much higher than ideal, as seen in Table 4.4. Note that repeatability was poorer in the elbow joint than in the shoulder. These two joints both use the same gear heads and similar gear ratios, however the elbow joint uses a belt drive. The added friction of the belt drive likely causes the poorer repeatability performance.

Table 4.4: Repeatability Results

Average Errors (μ rad) Using PID	Elbow	Shoulder
5 seconds	928	603
10 seconds	265	95

The deflection of the elbow and shoulder joints was measured experimentally. A small laser was clamped to the end of the manipulator, and a spot was projected onto a ruler taped to the wall. Different weights were suspended from the manipulator and the deflection of the arm was calculated. The control software for the arm was running so it could be verified that the encoder count remained constant and the motor did not move. The elbow joint was tested by itself, by supporting the upper arm underneath. Then both joints were tested together, and the stiffness of the shoulder joint was determined by using the data from the first test and the equation for two springs in series:

$$K_{total,series} = \frac{K_1 K_2}{K_1 + K_2} \tag{4.2}$$

The torsional stiffness of the gear head was estimated by taking another elbow stiffness test with enough weight to back drive the gear head, and holding the gear head output shaft fixed. This gave the stiffness for the joint without the gear head. The elbow stiffness was about 4 times lower than the lowest known stiffness, the intermediate gear shaft. This leads one to believe that the belt is the most flexible element in the joint. The shoulder joint stiffness is almost equal to the estimated gear head stiffness, while in theory it should be about 35% less due to significant deflection in the intermediate gear

shaft. These results will prove useful when samples can be manipulated. To do that, and end-effector is necessary.

5 End-Effector

5.1 Introduction

One of the main purposes of the manipulator arm is to acquire and manipulate rock samples. The arm therefore needs an end-effector to grasp rocks. The Sojourner rover did not have a manipulator, so no end-effectors have been tested yet on Mars. JPL is testing a multi-purpose end-effector on Rocky 7 (Volpe, 1998), which is another experimental test bed rover. JPL's end-effector, shown in use in Figure 5.1, is a two DOF tool that can dig, grasp, and point instruments. The double scoop can dig and pick up sand. If the two sides of the scoop are flipped around, they can be used to grasp rocks. Since the FSRL will not be doing digging work in the near future, an end-effector with such a diverse capability is not necessary for the experimental system.

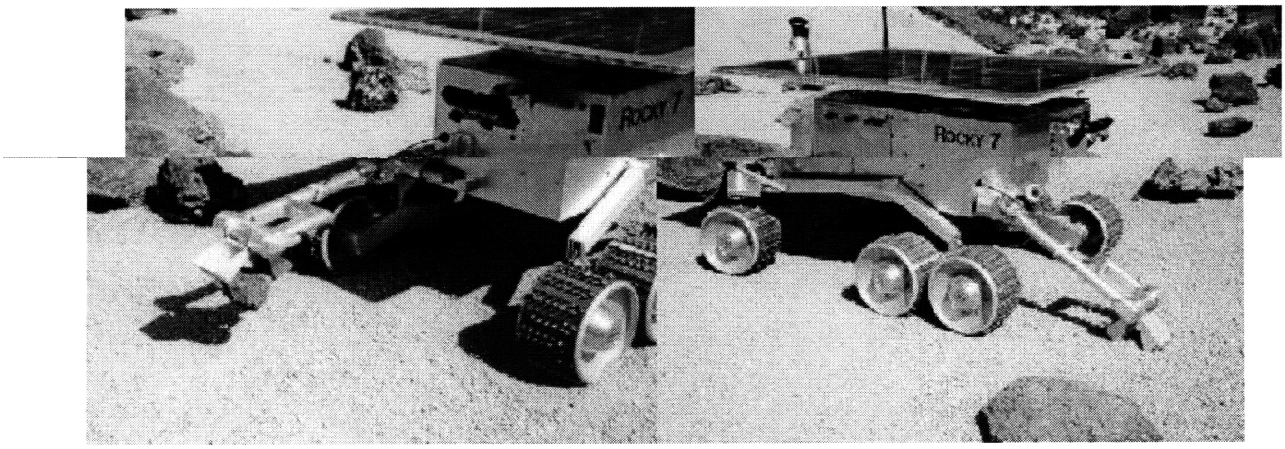

Figure 5.1: Rocky 7 with End-Effector (Volpe, 1998)

The first purpose of this end-effector research is to design and build an experimental test bed for manipulator control work. Part of this manipulator control work involves manipulation of rocks. The second purpose of this research, as mentioned

in Chapter 1, is to develop new, lightweight mechanisms to manipulate these rocks. Section 5.2 shows six new concepts for end-effector design, and selects the two most promising designs. Sections 5.3 and 5.4 detail the two best designs and section 5.5 presents some experimental results.

5.2 Concept Selection

There are three functional requirements for the end-effector. First, it must be light weight, which is a main goal of this mechanism design work. Second, it must be able to pick up rocks reliably, and third, it should be able to pick up a variety of rock sizes and weights. With these requirements in mind, six different end-effector concepts were generated. For purposes of weight, any actuation of the concepts is to be done by shape memory alloy wires.

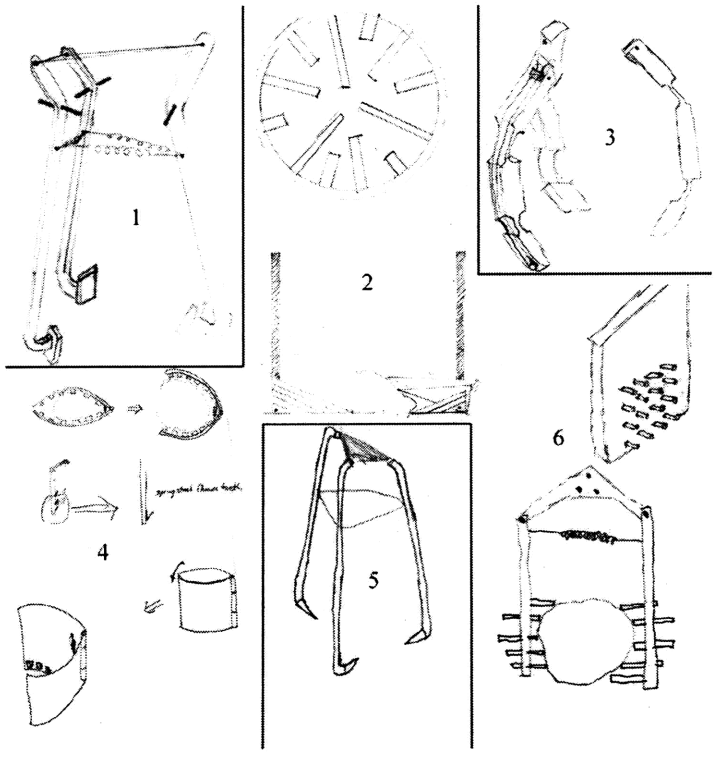

Figure 5.2: End-effector Concepts

Figure 5.2 displays these six concepts. Concept 1 uses three spring loaded rigid fingers, with compliant pads at the tips. SMA wires pull the fingers open, and the springs close the fingers when the wires cool. This configuration allows for short duration SMA use. Concept 5 is similar to concept 1, except that is uses three sharp metal points to contact the rocks instead of the pads. Concept 3 Uses three flexible fingers with the SMA's embedded in the fingers, which would be made of a polymer material. Concept 6 utilizes two plates that each have a matrix of spring loaded pins. These pins would be pushed up against the rock, forming the contour of the sample. Again, the plates would be spring loaded closed, and an SMA would be used for momentary opening of the plates. Concepts 2 and 4 take a different approach by not requiring actuation. Concept 2 is a hollow cylinder that contains many different sizes of pivoting teeth. When the device is pushed over the sample, some of the teeth lift up and then flip back down underneath the rock, and the rock can be lifted. To let go of the rock, the end-effector is turned upside down and the rock falls out the top. Concept 4 is similar to concept 2, except that it uses spring steel teeth that flex instead of pivot. Also, concept 4 uses essentially two halves of a cylinder that can be pushed open to accommodate a large variety of rock sizes.

All six concepts were rated based to ten different categories, as shown in Table 5.1. Each different criterion was given a weighting and five concepts were rated on a scale of 1 to 5 against Concept 1, which was chosen as the baseline concept. The category "Durable Materials" refers to the concepts' use of certain polymers. Low Martian temperatures can cause polymer flexures to become brittle, and the low atmospheric pressure causes degradation of some materials.

From the selection matrix, the two best designs emerged, concepts 4 and 5. Since these two designs have very different approaches to acquiring samples, both were built and tested.

Table 5.1: Concept Selection

						Concepts							
Selection Criteria	**Weigh**	**1**		**2**		**3**		**4**		**5**		**6**	
		3 Pads		**Ratchet Cup**		**Flexible Fingers**		**Ratchet Clamshell**		**3 Points**		**Contour Pins**	
	%	*Rating*	*Score*	*Rating*	*Score*	*Rating*	*Score*	*Rating*	*Score*	*Rating*	*Score*	*Rating*	*Score*
Sample Size Flexibility	5	3	0.15	1	0.05	3	0.15	2	0.1	3	0.15	2	0.1
Sample Shape Flexibility	15	3	0.45	2	0.3	4	0.6	3	0.45	3	0.45	3	0.45
Reliability of Grip	10	3	0.3	2	0.2	3	0.3	3	0.3	2	0.2	3	0.3
Creativity	10	3	0.3	5	0 5	4	0.4	4 5	0.45	3	0.3	4	0.4
Appearance	10	3	0.3	2	0.2	5	0.5	2.5	0.25	3.5	0.35	2.5	0 25
Durable Materials	5	3	0.15	5	0 25	1	0.05	2	0.1	4	0.2	4	0 2
Complexity	15	3	0.45	1	0.15	1	0.15	2	0.3	4	0.6	1	0.15
Actuation	15	2	0.3	5	0.75	1	0.15	5	0.75	2	0.3	2	0 3
Machining Time	5	3	0 15	2	0 1	1	0.05	2	0 1	3.5	0.175	1	0.05
Weight	10	3	0.3	3	0 3	3	0.3	3	0.3	3	0.3	2	0.2
Total Score		2.85		2.8		2.65		3.1		3 03		2 4	

5.3 Design 1

The first concept built was the three pointed fingers gripper. Each of the three fingers was made from 1/8" steel shaft. The fingers pivot about steel slip fit pins which are clamped onto the main plate by socket cap screws. The main plate is a circular piece of plastic, so that the fingers are electrically insulated. An elastomer was wrapped around the three fingers to serve as a spring. The SMA wires are tied through holes in the top of the fingers. The wires then run over Delrin guides and meet in the middle underneath the

plate. The wires are routed over the plate and back underneath to give more deformation length, allowing more finger travel. The Delrin guides provide low friction, insulated channels for the wires to follow. Figure 5.3 shows the design, with one of the wires and Delrin guides shown. An aluminum bracket bolted to the plate mates with the end of the manipulator. The 3 finger gripper is designed to be able to grasp rocks up to 2 ½" in diameter, and be able to hold the weight of a typical rock of that size. The end-effector weighs a remarkably light 2 ounces.

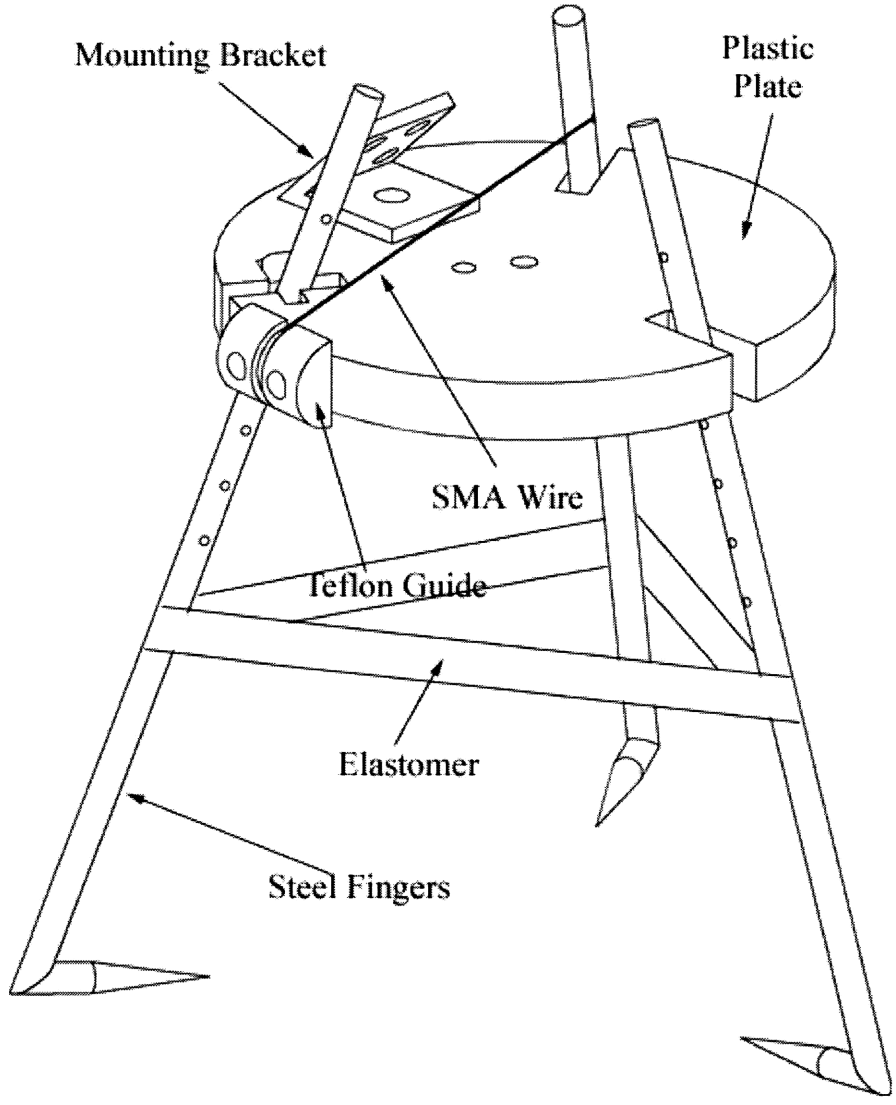

Figure 5.3: Three Fingers Design

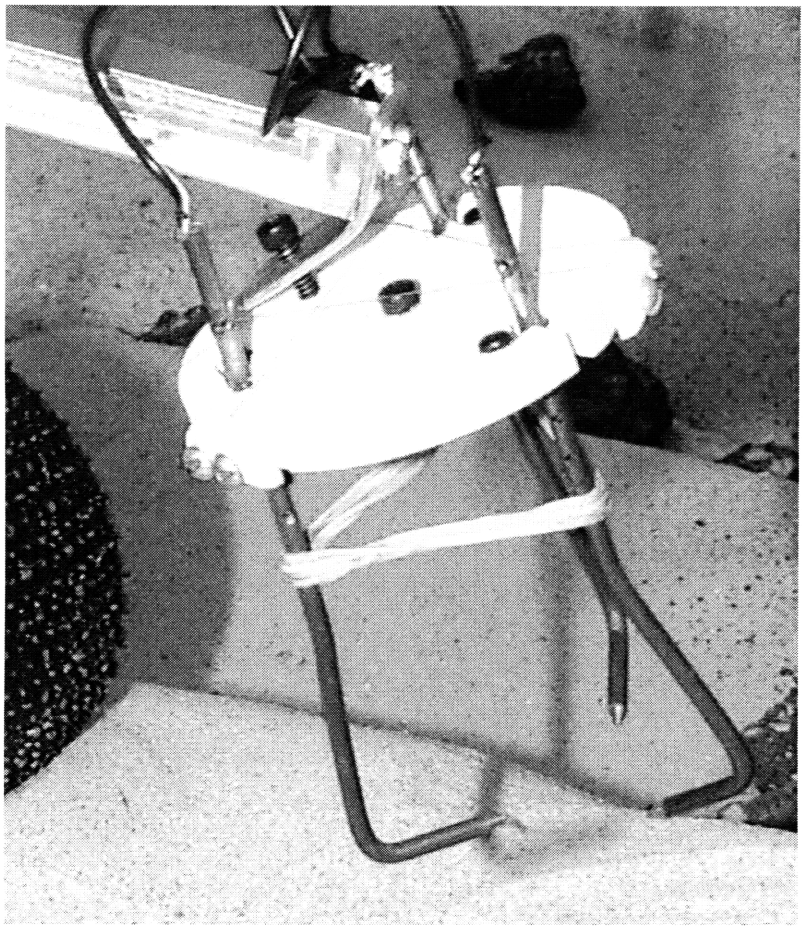

Figure 5.4: A Three Fingers Prototype Gripper

5.4 Design 2

The second concept to be constructed is the ratchet/clamshell design. Figure 5.5 shows the design. The two halves of the gripper are made of Lexan. Two spring steel beams support each half and hold it in the closed position, and the thickness of the beams can be varied to adjust the clamping force of the gripper. The flexible teeth are made of spring steel as well and are epoxied to the Lexan halves. The teeth are bent at a 135° angle so that as the gripper is pushed on top of a rock, the teeth and the halves are forced open. To release the sample, the gripper is turned upside down and the rock slides out the top. Again, an aluminum bracket bolted to the gripper mates with the end of the

manipulator. This end-effector is also designed to accommodate up to 2 ½" rock diameters and can be modified for SMA actuation if necessary. The end-effector weighs one ounce.

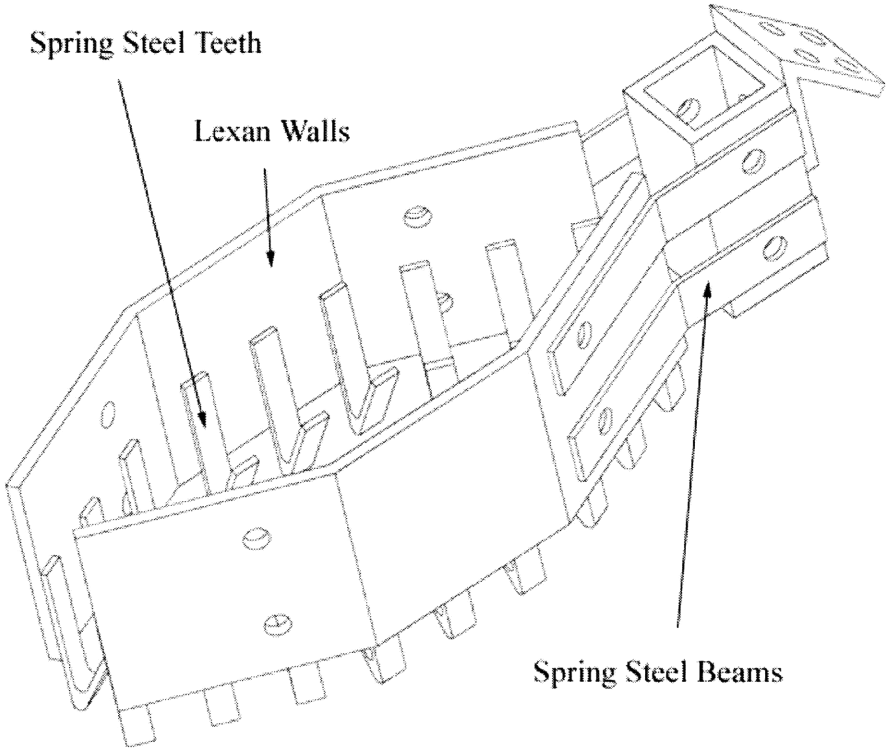

Figure 5.5: Ratchet Clamshell Design

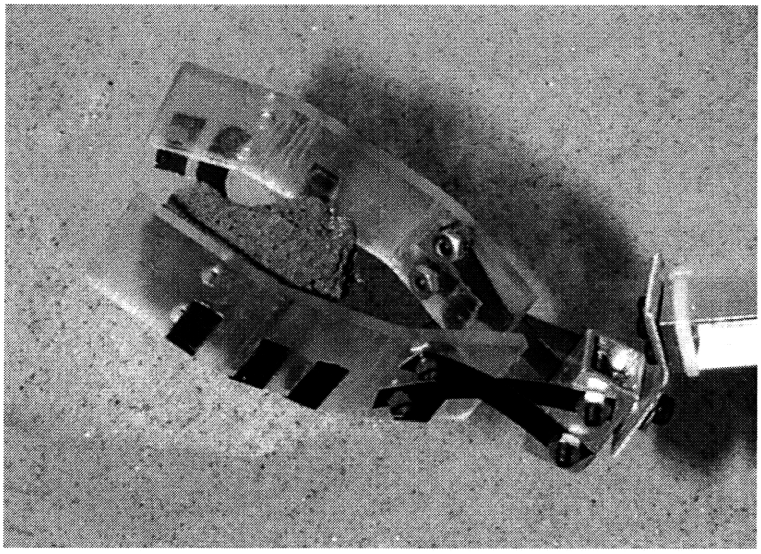

Figure 5.6: Ratchet Clamshell Prototype Gripper

5.5 Test Results

The two end-effectors were tested picking up rock samples. Two different kinds of rocks were used. Red volcanic lava rocks represent possible Mars samples. They are very porous and lightweight, being less dense than water. Silicon nuggets were also tested. They are much more dense, 2.33 g/cm^3, and have much smoother surface characteristics than the lava rocks. Figure 5.7 shows the two types of samples tested. Examination of Figures 1.1 and 1.2 suggests that many of the small rocks on mars will be partially buried in fine sand. Therefore, the lava and silicon rock samples were buried about halfway, as seen in Figure 5.8. The end-effectors were tested picking up a variety of samples of each kind of rock.

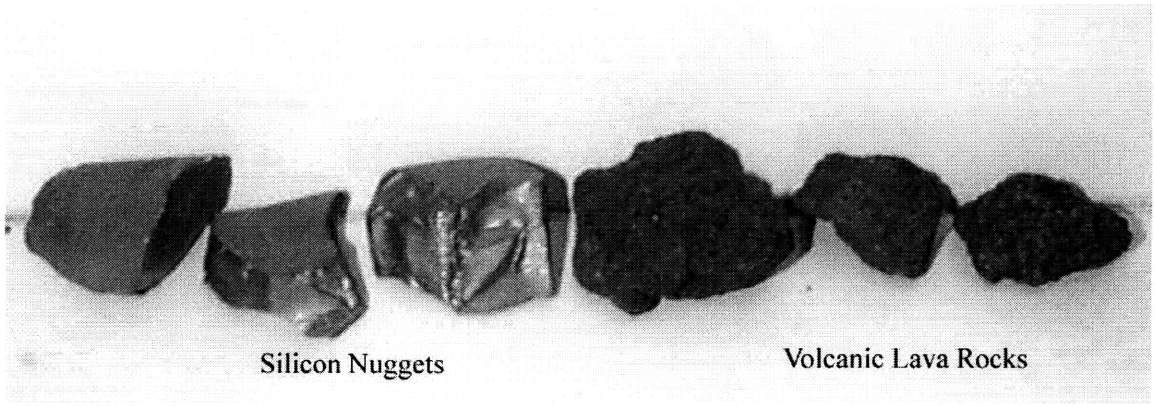

Figure 5.7: Test Samples

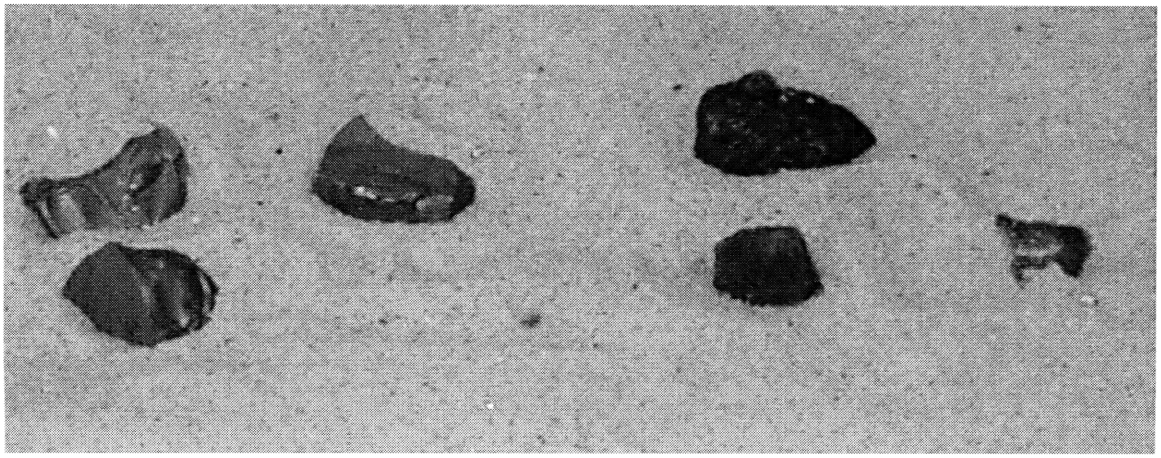

Figure 5.8: Sample Placement

The results of the tests are shown in Figure 5.9. If the rock was not picked up by the gripper in the first or second attempt, then it was considered a failure. For both end-effectors, the lava rocks proved to be easier to pick up, because they were lighter and had a rougher surface, which is easier to grip. The three finger gripper was very successful at probing into the sand, to reach the lower half of the samples. The samples that it usually failed at picking up were either of a long, thin shape or were heavy and had a very smooth, regular surface which was difficult to grip. The ratchet/clamshell gripper was the most successful at picking up the lava rocks. The only lava rocks that it had problems with were the ones that the gripper had to push deep into the sand to get a reasonable grip. This gripper didn't probe into the sand nearly as easily as the 3 finger end-effector. However, this end-effector had some problems picking up many of the silicon rocks because of their smooth surface. Often, the teeth would just slip right over the rock. Thus, surface texture seems to be an important factor in this end-effector's performance.

Figure 5.9: Test Results

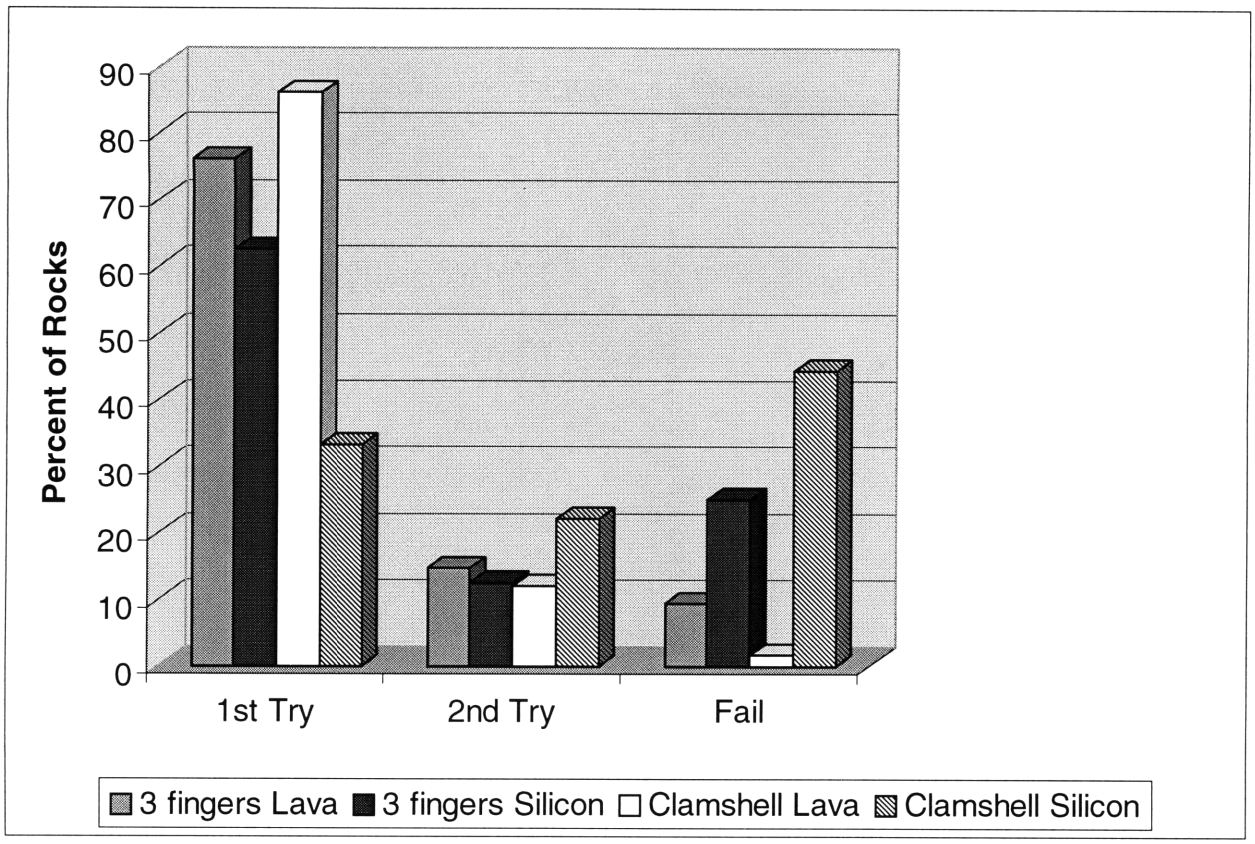
Percent of Rocks
90
80
70
60
50
40
30
20
10
0
1st Try
2nd Try
Fail
3 fingers Lava
3 fingers Silicon
Clamshell Lava
Clamshell Silicon

6 Conclusions and Future Work

6.1 Contributions of this work

This work has developed an experimental planetary rover system that will be used to evaluate mechanical designs and perform control, planning, vision and autonomy work with application to planetary exploration.

The six wheeled rover is lightweight and its geometry mimics JPL's lightweight survivable rover (LSR). The rover has high mobility, and facilitates the evaluation of different rover control techniques such as a fuzzy logic controller (Hacot, 1998). The reconfigurability mechanism demonstrates the use of shape memory alloys for rover reconfigurability. Position control within a couple of degrees was achieved. The manipulator arm is lightweight as well, and can exert a force of over half of the rover's weight. Deflection of the arm has been calculated, and repeatability tested as well. Finally, two different end-effectors were developed. These two grippers are substantially different from what is being used today. These ideas are lightweight and very effective at picking up lightweight rocks, as would be experienced in Martian gravity.

6.2 Future Work

The rocker bogie rover will continue to serve as an experimental test bed for further traction control studies, as well as planning, vision and autonomy. Wireless communication with the rover will eliminate the need for a tether, eliminating external forces on the rover from this tether. Reconfigurability is an issue that has just had its

surface scratched. The second generation design presented will be built and tested on the rover. Also, more robust control techniques can be implemented to improve performance. The manipulator arm performance needs to be improved as well. The friction in the joint gearing that has kept repeatability and response less than ideal is in fact a blessing. This friction will allow for friction compensation techniques using BSC control to be applied. Furthermore, compliance in the body of the rover allows for the investigation of manipulation from a compliant base. In order for this rover system to be used in a manner such as a rover on Mars would be, it needs to have improved on board sensing and control.

References

Ashby, M., Jones, D., *Engineering Materials 1, An Introduction to their Properties and Applications*, Pergamon Press, Oxford, 1980.

Ashby, M., *Materials Selection in Mechanical Design*, Butterworth-Heinemann, Oxford, 1992.

Bickler, D., "The New Family of JPL Planetary Surface Vehicles," *Proc. Intl. Symp. On Missions, Technologies, and Design of Planetary Mobile Vehicles*, pp. 301-306, Toulouse, France, September 28-30, 1992.

Bickler, D., *et al.*, "Technical Support Package On Planetary Microrover," *NASA Tech Brief from JPL New Technology Report,* Jet Propulsion Laboratory, Pasadena, CA, March, 1997.

Chottiner, J., *Simulation of a Six-Wheeled Martian Rover Called the Rocker-Bogie*, M.S. Thesis, The Ohio State University, Columbus, Ohio, 1992.

Duerig, T., *Engineering Aspects of Shape Memory Alloys*, Butterworth-Heinemann, London, 1990.

Farritor, S., Hacot, H., and Dubowsky, S. "Physics-Based Planning for Planetary Exploration." *1998 IEEE International Conference on Robotics and Automation*, Leuven, Belgium, May 1998.

Farritor, S., *Graduate Research Assistant*, Personal Communication, 1997-98.

Gilbertson, R., *Muscle Wires*, San Anselmo, CA, 1994.

Golombek, M. P., "Mars Pathfinder Mission and Science Results." *Proceedings of the 29th Lunar and Planetary Science Conference*, March 16-20, 1998.

Hacot, H., Dubowsky, S., and Bidaud, P. "Modeling and Analysis of a Rocker-Bogie Planetary Exploration Rover." *Twelth CISM-IFToMM Symposium*, Ro.Man.Sy. 98, Paris, July 1998.

Hacot, H., *Analysis and Traction Control of a Rocker-Bogie Planetary Rover*, M.Sc. Thesis, Mechanical Engineering Department, Massachusetts Institute of Technology, Cambridge, MA.

Iagnemma, K., Morel, G. and Dubowsky, S. "A Model-Free Fine Position Control Method Using the Base-Sensor: with Application to a Hydraulic Manipulator." *Proceedings of the Fifth IFAC Symposium on Robot Control: SYROCO 97*, Nantes, France, September 1997.

Liu, G., Iagnemma, K., Dubowsky, S. and Morel, G. "A Base Force/Torque Sensor Approach to Robot Manipulator Inertial Parameter Estimation." *1998 IEEE International Conference on Robotics and Automation*, Leuven, Belgium, May 1998.

Matijevic, J., "01 Surveyor Rover: Requirements, Constraints and Challenges," www.cs.cmu.edu/~metiorite/2001rover/, October 24, 1997.

Schenker, P., *et al.*, "Dexterous Robotic Sampling for Mars *in-situ* Science," *Intelligent Robotics and Computer Vision XVI* (Ed. D. Casasent et al.), SPIE Proc. 3208, 16 pp., Pittsburgh, PA Oct.14-17, 1997.

Schenker, P., *et al.* (2), "Lightweight Rovers for Mars Science Exploration and Sample Return," *Intelligent Robotics and Computer Vision XVI* (Ed. D. Casasent et al.), SPIE Proc. 3208, 13 pp., Pittsburgh, PA Oct.14-17, 1997.

Schenker, P., *et al.* (3), "A composite manipulator utilizing rotary piezoelectric motors: new robotic technologies for Mars in-situ planetary science," *Enabling Technologies: Smart Structures and Integrated Systems, Proc. SPIE SS97*, San Diego, CA, March, 1997.

Schildt, H., *Turbo C/C++: The Complete Reference*, McGraw Hill, 1992.

Small Parts Inc., 1997 Catalog, Miami Lakes, FL, 1997.

Troisfontaine, N., and Bidaud, P., "Optimal design of a Shape Memory Alloy actuator for Microgrippers." *Proc. of the Eleventh Symposium on Theory and Practice of Robots and Manipulators (Ro.ManSy'11)*, Udine, Italy, 1996.

Troisfontaine, N., Personal Communication, 1998.

Ulrich, K., Eppinger, S., *Product Design and Development*, McGraw-Hill Inc., New York, 1995.

Volpe, R., "Mobile Robot Manipulators for Mars Science." *Space Technology Journal*, 17(3-4), pp. 219-229, April 1998.

Youyi, C., Tu, H., "Shape Memory Materials '94," *Proceedings of the International Symposium of Shape Memory Materials*, Bejing, China, September 25-28, 1994.

Appendix A: Mars Data

Mass (kg)	6.42E+23
Mass (Earth = 1)	1.07E-01
Equatorial radius (km)	3,397.20
Equatorial radius (Earth = 1)	5.33E-01
Mean density (gm/cm^3)	3.94
Mean distance from the Sun (km)	227,940,000
Mean distance from the Sun (Earth = 1)	1.5237
Rotational period (hours)	24.6229
Rotational period (days)	1.025957
Orbital period (days)	686.98
Mean orbital velocity (km/sec)	24.13
Orbital eccentricity	0.0934
Tilt of axis (degrees)	25.19
Orbital inclination (degrees)	1.85
Equatorial surface gravity (m/sec^2)	3.72
Equatorial escape velocity (km/sec)	5.02
Visual geometric albedo	0.15
Magnitude (Vo)	-2.01
Minimum surface temperature	-140°C

Mean surface temperature	-63°C
Maximum surface temperature	20°C
Atmospheric pressure (bars)	0.007
Atmospheric composition	
Carbon Dioxide (C02)	95.32%
Nitrogen (N2)	2.70%
Argon (Ar)	1.60%
Oxygen (O2)	0.13%
Carbon Monoxide (CO)	0.07%
Water (H2O)	0.03%
Neon (Ne)	0.000250%
Krypton (Kr)	0.000030%
Xenon (Xe)	0.000008%
Ozone (O3)	0.000003%

Appendix B: Manipulator Motor/Gearhead/Encoder Data

	Torso Joint	Shoulder Joint	Elbow Joint
Motor	1624	1624	1616
Gearhead	16/8	16/7	16/7
Encoder	Magnetic HE	Magnetic HE	Magnetic HE

Motor	1616	1624
Max Speed (RPM)	12,000	12,000
Max Torque (oz-in)	0.11	0.21
Max Output Power (watts)	0.45	0.9
Armature Resistance (ohms)	83	24
Max Efficiency (%)	66	74
Stall Torque (oz-in)	0.13	0.599
Torque Constant (oz-in/amp)	0.922	1.224
Weight (oz)	0.43	0.74

Gearhead	16/7	16/8
Bearings	Shielded Ball	Shielded Ball
Max Radial Shaft Load (oz)	108	90
Max Axial Shaft Load (oz)	18	18
Backlash, unloaded (deg)	<1	0
Max Intermittant Output Torque (oz-in)	64	42.2
Weight	1.16	0.92
Ratio	134.00	262.00
Efficiency	60	43

Encoder	Magnetic HE
Output Waveform	Square Wave
Channels	2
Phase Shift (deg)	90
Pulses per Revolution	16
Power Requirement (mW)	25 mW
Max Signal Frequency (kHz)	7.2

Appendix C: Elbow and Shoulder Link Schematics

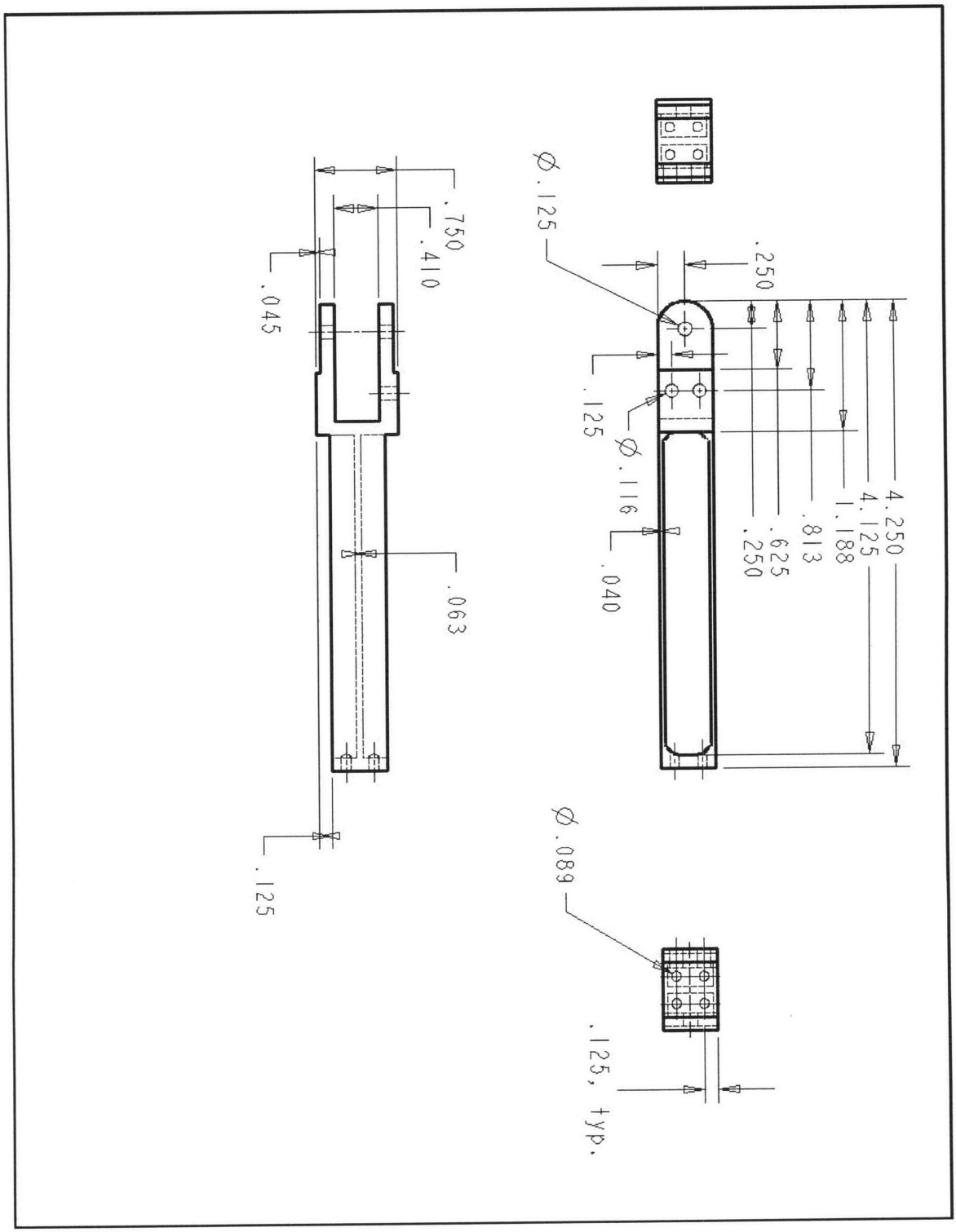

Figure C.1: Forearm Link

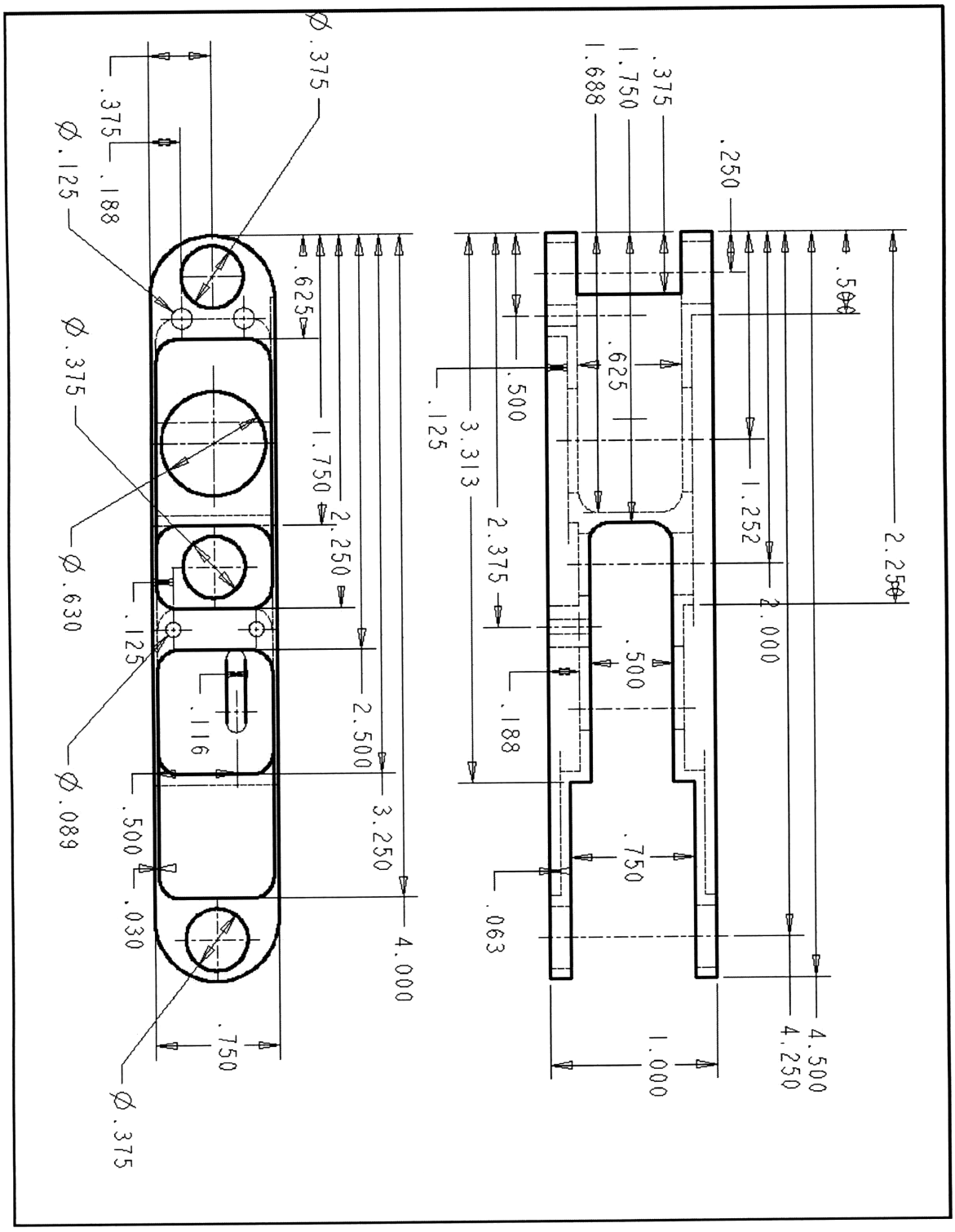

Figure C.2: Upper Arm Link